A STUDY OF IONOSPHERIC IRREGULARITIES

Technical Summary Report Contract AF 61(052)-500

by

H Bøen

P Christophersen

T Hagfors

FORSVARETS FORSKNINGSINSTITUTT
Norwegian Defence Research Establishment
P O Box 25 - Kjeller
Norway

AFCRL - 63 - 198

AD

AF EOAR 62 - 33
TR
10 March 1963

TECHNICAL SUMMARY REPORT

A STUDY OF IONOSPHERIC IRREGULARITIES

by

H Bøen
P Christophersen
T Hagfors

NORWEGIAN DEFENCE RESEARCH
ESTABLISHMENT, KJELLER, NORWAY
NDRE REPORT No 45

The research reported in this document has been sponsored in part by the Cambridge Research Laboratories, OAR, through the European Office, Aerospace Research, United States Air Force

Contents

FOREWORD

In the present summary report an account is given of theories and experiments designed to investigate the irregular structure of the ionosphere by studying the correlation between radio waves reflected at closely spaced frequencies. In part I of the report several different models are constructed of the ionosphere, and the relation between observable quantities on the ground and the properties of the ionospheric irregularities are derived. In part II of the report a set of experiments on reflections from the F-layer at closely spaced frequencies is described and the results of the observations are discussed in relation to the results of part I. Part III gives detailed description of the equipment used in the observations.

The work described is sponsored by the US Air Force through Office of Aerospace Research under contract AF-61(052)-500.

Part I

ON THE DESCRIPTION OF ELECTROMAGNETIC WAVES REFLECTED FROM A RANDOM MEDIUM

SUMMARY

Electromagnetic waves reflected from a random medium are described in terms of spatial correlation and of correlation between signals reflected at adjacent frequencies. The propagation of these correlation functions are studied both for limited and unlimited reflectors. Several different reflector models which could give rise to the random properties of the reflected waves are then discussed and various parameters are related to the observable correlation functions.

1 INTRODUCTION

Electromagnetic waves in passing through or being reflected from a spatially random medium such as the ionosphere are in many cases perturbed in a more or less random manner. A single plane wave passing through such a medium will often lose its plane wave character and develop into an angular spectrum of waves. Similarly a short pulse passing through such a medium will be widened out because of the irregularities. Often the medium might also vary with time and the wave passing through becomes time varying. This means that a wave which initially consists of a single spectral line gradually will develop into a frequency spectrum. All of these perturbations may also be described in a different way. A wave which is initially coherent over a large spatial area will lose this coherence as the wave is progressing through a random medium. The definite phase and amplitude relationship initially existing in a modulated wave will gradually vanish with the wave travelling through a random medium. With a time varying medium, the relation of fields separated by a time interval will become washed out as the wave penetrates into the random medium.

The random nature of the diffracting medium will only permit a statistical description of the components of the wave-fields. The different field components will be functions of position in space $\vec{r}$, of time t and of the frequency ω of the applied signals. In this report we describe the field components by means of a covariance relating the fields observed at spatial distances $\Delta\vec{r}$ and at frequencies separated by $\Delta\omega$. In what follows we mostly leave out the description of the effects of the random time variation and thus only deal with a covariance being a function of $(\Delta\vec{r},\Delta\omega)$.

For signals reflected from the ionosphere the space and time correlations have been extensively studied (1, 2, 3). Often the interpretation is rather difficult in that the size, shape and location of the irregularities in the medium giving rise to the random field cannot be deduced without a considerable amount of additional hypotheses. For signals transmitted through the ionosphere from radio stars or earth satellites the interpretation of the wave structure is considerably less ambiguous (1, 4, 5, 6). Important data have been obtained on ionospheric irregular structure from such observations. In view of the many unsettled questions concerning the reflection mechanism and the irregular structure in the ionosphere, it appears that new observational techniques should be attempted in order to provide additional or supplementary information. One of these techniques might be the correlation of signals reflected at spaced frequencies, or alternatively, the study of the distortion of extremely short pulses reflected from the ionosphere. Attempts in this direction have been made before, but the interpretation of previous data might be of doubtful validity (7).

In this part of the report, therefore, we want to study theoretically the relationship between space and frequency correlation functions for several different models of the irregular structure of the ionosphere. We are in particular attempting to examine to what extent the frequency correlation technique could provide additional information on

the ionospheric structure and under which circumstances this be the case. Section 2 below therefore deals with some general properties of the statistical functions of the wave-field. Section 3 discusses the relation between the properties of the wave-field and the structure of the irregular medium for a number of different models.

2 DESCRIPTION OF THE DIFFRACTED FIELD

In this section we give a brief description of the properties of the random diffracted field. We assume that the field is given over a screen at $z = o$ and that field variations only take place in the x-direction, hence the field is one-dimensional. We furthermore assume that a statistical ensemble of such random screens are given and that the statistical properties of the ensemble is given. The actual physical mechanism giving rise to the random field distributions over the screen is not discussed here. Certain simple models are dealt with in the next section. Knowing the statistical properties of the field in the plane $z = 0$ we inquire about the propagation of these properties into the half plane $z > 0$. This approach has been used by J A Ratcliffe (8) and it has been extended by others. Our main excuse for repeating some of the already known arguments here is that we also want to include in our discussion the relation of two harmonically varying fields at slightly different frequencies. The two cases of an infinitely extended screen and that of a spatially limited one are considered separately.

2.1 Covariance for infinite screen

Let the field over the screen at $z = 0$ and at a frequency ω be denoted by $g(x,0,\omega)$. This field can be expressed in terms of an angular spectrum $F(S,\omega)$ through (8):

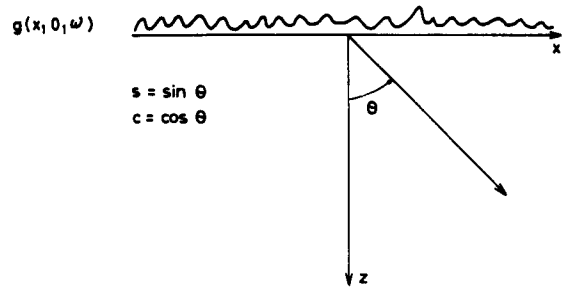

Figure 2.1 Geometry of the diffraction problem

$$g(x,0,\omega) = \int F(S,\omega) \exp\{ i \tfrac{\omega}{c} S x \} dS \qquad (2.1)$$

which implies that:

$$F(S,\omega) = \tfrac{\omega}{2\pi c} \int g(x,0,\omega) \exp\{ -i \tfrac{\omega}{c} S x \} dx \qquad (2.2)$$

where $S = \sin\theta$ and where c = velocity of the waves. The field at any point below the screen, i.e. at $z > 0$ can be expressed as:

$$g(x,z,\omega) = \int_{-\infty}^{+\infty} F(S,\omega) \exp\{ i \tfrac{\omega}{c} (Sx + Cz) \} dS \qquad (2.3)$$

where $C = \sqrt{1 - S^2} = \cos\theta$. This simply means that the field in front of the screen is expressed by means of the field at the screen itself - Huygens prinsiple. For simplicity we assume that the field is normalized in such a way that $\left\langle |g(x,z,\omega)|^2 \right\rangle_{av}$ is equal to unity. The bracket $\left\langle \quad \right\rangle_{av}$ means assembly average. It should be noted that the assembly averaging employed here is not the same as that used by Ratcliffe (8) who averages over x. When the properties of the field vary in the x-direction the two types of averaging will give different results. It is thought that the assembly averaging in some situations

corresponds more closely to the actual physical problem under study, see also (9).

The nature of the random field will now be described in terms of the complex correlation coefficient $R(\Delta x,\Delta\omega,z)$ defined by:

$$R(\Delta x,\Delta\omega,z) = \left\langle g^{*}(x,z,\omega)\ g(x+\Delta x,z,\omega+\Delta\omega)\right\rangle_{av} \qquad (2.4)$$

where the asterisk denotes the complex conjugate. At the screen the statistical properties should be obtained by putting $z = 0$.

In order to relate the correlation at the screen to the correlation at some point in front of the screen we observe that:

$$g(x,z,\omega) = \frac{\omega}{2\pi c}\int dS \int d\xi\ g(\xi,0,\omega)\ \exp\{\, i\,\frac{\omega}{c}\,[S(x-\xi)+Cz]\} \qquad (2.5)$$

which follows from a combination of formulae (2.1) - (2.3). We therefore find:

$$R(\Delta x,\Delta\omega,z) = \frac{\omega(\omega+\Delta\omega)}{(2\pi c)^2}\iiint dSdS'd\xi d\xi'\left\langle g^{*}(\xi,0,\omega)g(\xi',0,\omega+\Delta\omega)\right\rangle_{av}\cdot$$

$$\cdot\ \exp\{\, -i\,\frac{\omega}{c}\,[S(x-\xi)+Cz] + i\,\frac{\omega+\Delta\omega}{c}\,[S'(x+\Delta x-\xi')+C'z]\} \qquad (2.6)$$

Because the statistical properties of the field at the screen are independent of position, the average under the integral sign only depends on the difference $\rho = \xi' - \xi$. Integration over ξ therefore gives:

$$R(\Delta x,\Delta\omega,z) = \frac{\omega(\omega+\Delta\omega)}{2\pi\cdot\sigma^2}\iiint dSdS'd\rho\ R(\rho,\Delta\omega,0).\delta(\frac{\omega S}{c} - \frac{\omega+\Delta\omega}{c}S')\cdot$$

$$\exp\{\, -i\,\frac{\omega}{c}\,(Sx+Cz) + i\,\frac{\omega+\Delta\omega}{c}[S'(x+\Delta x-\rho) + C'z]\} \qquad (2.7)$$

where $\delta(\ )$ is a Dirac delta-function. Different components in the angular spectrum therefore contribute at the two frequencies, viz.:

$$S' = \frac{\omega}{\omega+\Delta\omega} S \tag{2.8}$$

Carrying out the integration over S' in (2.7) leaves us with a double integral for the correlation coefficient:

$$R(\Delta x,\Delta\omega,z) = \frac{\omega}{2\pi c} \int dS \exp\{ i\frac{\omega}{c} S\cdot\Delta x + i\frac{z}{c}(C'(\omega+\Delta\omega) - C\cdot\omega) \}$$

$$\cdot \int d\rho\ R(\rho,\Delta\omega,0) \exp(-iS\rho \frac{\omega}{c}) \tag{2.9}$$

Let us now examine two special cases, the first being $\Delta\omega = 0$. In this case:

$$R(\Delta x,z) = \frac{\omega}{2\pi c} \iint dSd\rho\ R(\rho,0,0) \exp\{ i\frac{\omega}{c} S(\Delta x-\rho)\} = R(\Delta x,0,0) \tag{2.10}$$

The spatial correlation therefore remains invariant with increasing distance from the screen, as is well known (8). In the second case $\Delta x = 0$ and we obtain:

$$R(\Delta\omega,z) = \frac{\omega}{2\pi c} \iint dSd\rho\ R(\rho,\Delta\omega,0) \exp\{-i\frac{\omega}{c} S\rho + i\frac{z}{c}(C'(\omega+\Delta\omega)-C\omega)\} \tag{2.11}$$

It can be seen that this expression does vary as the distance z is increased. The explanation for the variation of frequency correlation with distance z is best seen as follows. With increasing z the exponential will become more and more rapidly oscillating function of $\Delta\omega$. Eventually contributions will only arise when $\Delta\omega \simeq 0$ in the correlation function, hence:

$$R(\Delta\omega,z) \to \int dS\ \exp\{i\tfrac{z}{c}(C'(\omega+\Delta\omega)-C\omega)\} \cdot \tfrac{\omega}{2\pi c} \int d\rho\ R(\rho,0,0)\ \exp\{-i\tfrac{\omega}{c}S\rho\}$$

(2.12)

The last part of this is equal to the angular power spectrum at the frequency ω. Expanding furthermore the first exponent to first order in $\Delta\omega$ we find:

$$R(\Delta\omega,z) \to \int dS\ \left\langle |F(S,\omega)|^2 \right\rangle_{av} \exp\{\, i\ \frac{\Delta\omega \cdot z}{c\sqrt{1-S^2}}\ \} \qquad (2.13)$$

In this asymtotic form the result is fairly easy to understand if it is rederived in a different way by making use of the relation between the average power pulse response (or "delay spectrum") $D(\tau)$ and the correlation function $R(\Delta\omega)$. Here τ represents the delay of the network which is equivalent to the propagation circuit. The relation is (10):

$$R(\Delta\omega) = \int D(\tau) \exp\{\, i\Delta\omega\cdot\tau\ \}\, d\tau \qquad (2.14)$$

which is valid as long as $(\Delta\omega/\omega) << 1$. This is also the condition for (2.13) to be valid.

In Figure 2.1 it is seen that the delay τ is given by

$$\tau = \frac{z}{c}\frac{1}{\sqrt{1-S^2}} \qquad (2.15)$$

Substitution into (2.14) gives:

$$R(\Delta\omega,z) = \int dS\{\frac{z}{c}\frac{S}{(\sqrt{1-S^2})^3}\, D(\frac{z}{c\sqrt{1-S^2}})\}\ \exp(i\ \frac{\Delta\omega z}{c\sqrt{1-S^2}})$$

(2.16)

Identification of the expression within the curly brackets with the angular power spectrum brings this into agreement with (2.13). The interpretation is now clear: with increasing distance from the screen and with an opening angle in the power spectrum which does not change with distance the spread in time delays is increasing and the frequency correlation range narrows. At the same time this suggests that with a source which is limited in extent the frequency correlation might not change much. This is examined in detail below.

2.2 Covariance for finite screen

Let us next assume that the random diffraction fields are viewed through a slit at $z = 0$ which extends from $x = -\frac{W}{2}$ to $x = \frac{W}{2}$, and that the statistical properties are independent of position within the slit. We furthermore assume that the scale of the irregularities is much smaller than the width of the slit. Under these assumptions we find that equation (2.6) must be replaced by:

$$R(\Delta x,\Delta\omega,z) = \frac{\omega(\omega+\Delta\omega)}{(2\pi c)^2}\int_{-\frac{W}{2}}^{+\frac{W}{2}} d\xi \int d\rho R(\rho,\Delta\omega,0)\iint dSdS' \exp\{-i\tfrac{\omega}{c}[S(x-\xi)+Cz]+$$

$$+ i\tfrac{\omega+\Delta\omega}{c}[S'(x+\Delta x-\xi-\rho) + C'z]\} \qquad (2.17)$$

Because of the limited extent of the source the fields will die out with distance from the screen and the above correlation function will <u>not</u> be normalized as in the case of an infinite screen. Integration over S and S' gives the unnormalized correlation:

$$R(\Delta x,\Delta\omega,z) = \frac{1}{2\pi c\cdot z}\sqrt{\omega(\omega+\Delta\omega)}\exp\{i\tfrac{\Delta\omega\cdot z}{c}\}\int d\rho\ R(\rho,\Delta\omega,0)$$

$$\exp\{i\tfrac{\omega}{2cz}(\Delta x-\rho)^2\}\int d\xi\ \exp\{i\tfrac{\omega}{cz}[(x-\xi)(\Delta x-\rho)+\tfrac{\Delta\omega}{2\omega}(x-\xi)^2]\}$$

(2.18)

The interpretation of this is most convenient if we consider the same two special cases as above, viz. those of $\Delta x = 0$ and $\Delta\omega = 0$. When $\Delta\omega = 0$:

$$R(\Delta x,z) = \frac{1}{\pi}\int d\rho\ R(\rho,0)\ \exp\{i\frac{\omega}{2zc}[(\Delta x-\rho)^2+2x(\Delta x-\rho)]\}\ \frac{\sin\frac{\omega W}{2cz}(\rho-\Delta x)}{(\rho-\Delta x)} \tag{2.19}$$

Here we see that when $W \to \infty$ with z constant the sine term will tend to a δ-function and contributions to the last integral will only arise where $\rho = \Delta x$, and it will be found that $R(\Delta x,z)$ will be constant and the same as at the screen. When we let $z \to \infty$ with W constant, the integral will become a more and more slowly varying function of Δx. The distance in space over which the correlation remains high therefore increases with distance from the screen. Note that this applies to a finite screen and with ensemble averaging!

When $\Delta x = 0$:

$$R(\Delta\omega,z) \equiv \frac{W}{2\pi cz}\sqrt{\omega(\omega+\Delta\omega)}\ \exp\{\,i\,\frac{\Delta\omega\cdot z}{c}\,(1+\tfrac{1}{2}(\tfrac{x}{z})^2)\}\cdot$$

$$\cdot\int d\rho\ R(\rho,\Delta\omega,0)\ \exp\{\,i\,\frac{\omega}{2cz}\,(\rho^2-2x\rho)\} \tag{2.20}$$

In performing the integration we had to assume that W^2 is small compared with $8z(\frac{c}{\Delta\omega})$. Here, as $z \to \infty$, apart from the rapidly oscillating phase factor outside the integral the frequency correlation tends to become constant and independent of z.

The conclusion from this section can therefore be stated briefly as follows:

For an infinite screen the space correlation is independent of distance from the screen whereas the frequency correlation narrows. For a finite screen the space correlation widens out with distance from the

screen whereas the frequency correlation tends towards an asymptotic value with z only determined by the properties of the correlation on the screen.

An extension to a two-dimensional screen is simple in principle, but it is not carried out here because it does not appear that any essentially new points of physical interest are brought out thereby.

3 THE ORIGIN OF THE RANDOM WAVE FIELD

In the previous section we assumed the field variations to be described statistically at some plane $z = 0$. We then went on to study the propagation of these properties away from the screen. - In the present section we must inquire about the different physical mechanisms which could give rise to the random field variations over the reference screen. Because we want to consider waves reflected from the ionosphere we do not discuss the problem of a wave being transmitted through an irregular medium which would be appropriate in the case of radio star or earth satellite studies. The problem of reflection from an irregular medium is so complex that we must try to construct models which are simple enough to be discussed without too much difficulty, yet sufficiently detailed to convey some of the features of the actual reflection mechanism. Two types of models will be considered. The first type is a surface model. The waves are regarded as being reflected from randomly corrugated surfaces with reflection coefficient unity. The second type is a volume mechanism where irregularities in electron density are embedded in the ionospheric layer below the reflection level. The irregularities are considered as weakly scattering.

For simplicity we consider only an incident plane wave at vertical incidence on the ionosphere. An arbitrary incident wave can be constructed from an angular spectrum of such plane waves.

3.1 Reflection from a single corrugated surface

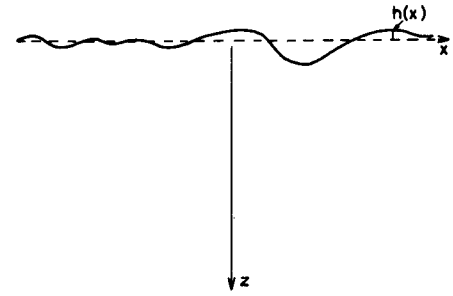

Figure 3.1 Reflection from corrugated surface

Consider the surface shown in Figure 3.1. The random corrugations are in the x-direction only and the function $h(x)$ describes the deviation of the surface from its mean position.

Provided the surface gradients are not too steep and the structure of the surface too small, the field referred to $z = 0$ which is the mean position of the screen becomes:

$$g(x,0,\omega) = \exp\{ - i \frac{\omega}{c} \cdot 2h(x) \} \qquad (3.1)$$

It is implied that the incoming plane waves are of unit amplitude and that the reflection coefficient of the surface is unity. The correlation function at the screen becomes:

$$R(\Delta x,\Delta\omega,0) = \left\langle \exp\{ i \frac{2}{c}(\omega h(x) - (\omega+\Delta\omega)\, h(x+\Delta x))\} \right\rangle_{av} \qquad (3.2)$$

In order to make some progress with this it will be assumed that $h(x)$ and $h(x+\Delta x)$ are distributed in accordance with a joint normal distribution with the following parameters:

$$\left\langle h(x)^2 \right\rangle_{av} = \left\langle h(x+\Delta x)^2 \right\rangle_{av} = h_m^2$$

$$\left\langle h(x) \right\rangle_{av} = \left\langle h(x+\Delta x) \right\rangle_{av} = 0 \qquad (3.3)$$

$$\left\langle h(x)h(x+\Delta x) \right\rangle_{av} = h_m^2 \, \rho(\Delta x)$$

With these assumptions it follows that:

$$R(\Delta x,\Delta\omega,0) = \exp\{-(\frac{2h_m}{c})^2(\omega(\omega+\Delta\omega)(1 - \rho(\Delta x)) + \frac{(\Delta\omega)^2}{2})\} \qquad (3.4)$$

For $\Delta\omega = 0$ this simplifies to

$$R(\Delta x,0,0) = \exp\{ - (\frac{2\omega h_m}{c})^2(1 - \rho(\Delta x))\} \qquad (3.5)$$

and this is the same as the correlation at the ground in the case of ionospheric reflections provided the aerial polar diagram is not so narrow that the screen appears as if limited. The result (3.5) is well known from previous investigations (11). We now have to decide upon a specific form of the correlation function $\rho(\Delta x)$ at the reflecting surface before further progress can be made. For lack of specific information we make the convenient choice $\rho(\Delta x) = \exp(-\Delta x^2/l^2)$ where l is the scale of the corrugations. The joint correlation function at the receiver then becomes, see (2.9):

$$R(\Delta x,\Delta\omega,z) = \frac{\omega}{2\pi c} \exp(- 2(\frac{h_m\Delta\omega}{c})^2) \int dS$$

$$\exp\{i \frac{\omega}{c} S\cdot\Delta x + i \frac{z}{c}(C'(\omega+\Delta\omega) - C\omega)\} \cdot$$

$$\cdot \int d\xi \, \exp\{-(\frac{2h_m}{c})^2[\omega(\omega+\Delta\omega)(1 - \exp(-\xi^2/l^2))]\} \cdot$$

$$\exp(- i S\xi \frac{\omega}{c}) \qquad (3.6)$$

We now distinguish between the case of a deep reflector, or $h_m > \lambda$, and a shallow reflector, $h_m < \lambda$.

It is convenient here and in what follows to introduce the r.m.s. opening angle θ_m of the angular power spectrum to simplify the formulae. In the case of a deep reflector we find approximately that:

$$\theta_m^2 \approx 8 \left(\frac{h_m}{l}\right)^2 \tag{3.7}$$

Introduction of this in formula (3.6) gives, still for a deep reflector:

$$R(\Delta x,\Delta\omega,z) = \frac{\exp\{ i\frac{z\Delta\omega}{c} - 2(\frac{h_m\Delta\omega}{c})^2\}}{\sqrt{1 - i\,\theta_m^2\cdot\frac{z}{c}\Delta\omega(1+\frac{\Delta\omega}{\omega})}}$$

$$\exp\{ \frac{-\frac{1}{2}\,\theta_m^2\,\frac{\omega(\omega+\Delta\omega)}{c^2}\,\Delta x^2}{1 - i\,\theta_m^2\,\frac{z}{c}\Delta\omega(1+\frac{\Delta\omega}{\omega})} \} \tag{3.8}$$

When $\Delta\omega = 0$ this reduces to:

$$R(\Delta x,z) = \exp\{ -\tfrac{1}{2}\,\theta_m^2\,(\tfrac{\omega}{c})^2\,\Delta x^2 \} \tag{3.9}$$

which is also a reasonable approximation for $R(\Delta x,0)$ in this particular case.

When $\Delta x = 0$ and when phase factors are neglected we have:

$$R(\Delta\omega,z) = \frac{1}{\sqrt{1 - i\,\theta_m^2\,\frac{z}{c}\Delta\omega(1+\frac{\Delta\omega}{\omega})}}\exp\{ -2(\tfrac{\Delta\omega}{c})^2\,h_m^2 \} \tag{3.10}$$

The first factor which is due to the angular spectrum of waves comprising the total signal drops to half of its magnitude at $\Delta\omega = 0$ when:

$$\theta_m^2\,\frac{z}{c}\,\Delta\omega = \sqrt{3}$$

or when:

$$\Delta\omega_z = \frac{\sqrt{3}}{\theta_m^2} \cdot \frac{c}{z} \tag{3.11}$$

The exponential factor, on the other hand drops to about one half when

$$2(\frac{\Delta\omega}{c})^2 \cdot h_m^2 = 1$$

or when

$$\Delta\omega_c = \frac{1}{\sqrt{2}} \cdot \frac{c}{h_m} \tag{3.12}$$

For this model it is well known that the observation of spatial correlation only gives information on the ratio (h_m/l). If the frequency correlation is to provide additional information we must require that:

$$\Delta\omega_c < \Delta\omega_z$$

which means that:

$$z < \sqrt{6} \frac{h_m}{\theta_m^2} \tag{3.13}$$

In the other case, that of a shallow reflector, the r.m.s. opening angle for the random part of the spectrum becomes:

$$\theta_m^2 = 2 \cdot \frac{c^2}{(\omega l)^2} \tag{3.14}$$

The joint correlation function at distance z from the screen in this approximation again from formula (3.6) becomes:

$$R(\Delta x,\Delta\omega,z) = \exp\{\, i\,\frac{\Delta\omega z}{c} - 2(\frac{\Delta\omega h_m}{c})^2 \,\}$$

$$(1 - (\frac{2h_m}{c})^2\omega(\omega+\Delta\omega)\{1 - \frac{\exp\{-(\frac{\Delta x}{l})^2 \frac{1}{1-i\theta_m^2\frac{z}{c}\Delta\omega}\}}{\sqrt{1 - i\,\theta_m^2\,\frac{z}{c}\,\Delta\omega}}\})$$

(3.15)

which for $\Delta\omega = 0$ reduces to:

$$R(\Delta x,z) = \{1 - (\frac{2h_m\omega}{c})^2(1 - \exp\{ - (\frac{\Delta x}{l})^2 \})\} \qquad (3.16)$$

We therefore see that the correlation does not drop to zero, but to a value determined by the depth h_m, and that the width is determined only by the scale of the corrugations l. When $\Delta x = 0$ we obtain:

$$R(\Delta\omega,z) = \exp\{ - 2(\frac{\Delta\omega h_m}{c})^2 + i\,\frac{\Delta\omega}{c}\,z \,\}$$

$$\{1 - (\frac{2h_m}{c})^2\omega(\omega+\Delta\omega)\{1 - \frac{1}{\sqrt{1 - i\,\theta_m^2\,\frac{z}{c}\,\Delta\omega}}\}\} \qquad (3.17)$$

Because $\frac{\Delta\omega}{\omega} << 1$ and since $\frac{\omega h_m}{c} < 1$ by assumption, the first exponential factor is very close to unity. The width of the random part of the returned waves is simply determined by the width of the angular power spectrum, and no more information can be obtained from frequency correlation than from space correlation.

3.2 Reflection from two corrugated screens

We next imagine the reflection at the two frequencies to take place at different surfaces corresponding to the deeper penetration into the ionosphere by the higher frequency wave. We make the very crude assumption that both waves travel undisturbed up to their reflection

level, and that the reflection occurs with a reflection coefficient of unity. We furthermore take the electron density in the mean to be a linear function of height z, viz.:

$$N(z) = -g(z - z_o) \qquad z < z_o \qquad g > 0 \tag{3.18}$$

(note that z is positive downwards!). The difference in mean height of reflection caused by the frequency change $\Delta\omega$ becomes:

$$\Delta z = -\frac{2M\epsilon_o}{ge^2}\,\omega \cdot \Delta\omega = -A\,\Delta\omega \tag{3.19}$$

Each of the two reflecting surfaces are regarded as being described statistically in the same way as the single surface in the previous section, and both with the same statistical parameters. The two surfaces are not identical, but differ more and more with increasing mean separation Δz. In this case we let the deviations from the mean heights be denoted by:

$$\begin{aligned} &h(x,z) \quad \text{at height } z \\ &h(x,z+\Delta z) \quad \text{at height } z+\Delta z \end{aligned} \tag{3.20}$$

and we take the relation between the height deviations to be:

$$\Big\langle h(x,z)\; h(x+\Delta x, z+\Delta z)\Big\rangle_{av} = h_m^{\,2}\,\rho(\Delta x, \Delta z) \tag{3.21}$$

The situation is illustrated in Figure 3.2 showing three different surfaces. For convenience the reference plane is now chosen at the mean height of reflection for the lower frequency.

For plane waves of unit amplitude we obtain for the reflected fields at the reference plane $z = 0$.

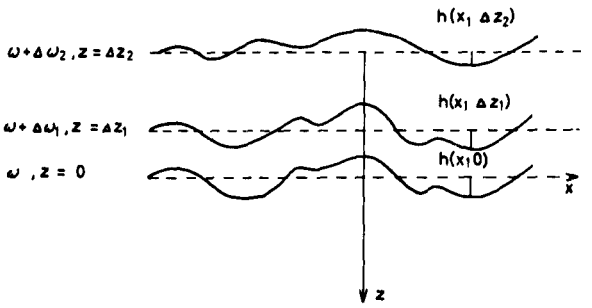

Figure 3.2 Reflection from two corrugated surfaces

$$g(x,0,\omega) = \exp\{ - i \frac{\omega}{c} 2\, h(x,0) \}$$

and

$$g(x,0,\omega+\Delta\omega) = \exp\{ - i \frac{\omega+\Delta\omega}{c} 2(h(x,\Delta z) - \Delta z) \} =$$

$$= \exp\{ - i \frac{\omega+\Delta\omega}{c} 2(h(x,\Delta z) + A\cdot\Delta\omega)\} \qquad (3.22)$$

For the complex correlation at the reference plane we now obtain:

$$R(\Delta x,\Delta\omega,0) = \exp\{ - 2i \frac{\omega+\Delta\omega}{c} \Delta z \} \cdot$$

$$\exp\{ -(\frac{2h_m}{c})^2 [\omega(\omega+\Delta\omega)(1-\rho(\Delta x,A\Delta\omega)) + \frac{\Delta\omega^2}{2})\} \qquad (3.23)$$

Again we have to make an assumption about the correlation function $\rho(\Delta x,\Delta z)$ in order to make further progress. We arbitrarily put:

$$\rho(\Delta x,\Delta z) = \exp\{ - (\frac{\Delta x^2}{l^2} + \frac{\Delta z^2}{m^2}) \} \qquad (3.24)$$

where m must be interpreted as a vertical scale. Distinguishing again between deep and shallow reflectors as before one finds:

For deep reflector:

$$R(\Delta x,\Delta\omega,z) = \exp\{ i (2 \frac{\omega+\Delta\omega}{c} \Delta z + \frac{\Delta\omega \cdot z}{c})\}$$

$$\exp\{ - 2(\frac{h_m}{c})^2(1 + 2 \frac{A^2\omega(\omega+\Delta\omega)}{m^2}) \Delta\omega^2 \} \cdot$$

$$\frac{1}{\sqrt{1 - i \theta_m^2 \frac{z}{c} \Delta\omega(1 + \frac{\Delta\omega}{\omega})}}$$

$$\exp\{ - \frac{\frac{1}{2} x^2 \cdot \theta_m^2 \cdot \frac{\omega(\omega+\Delta\omega)}{c^2}}{1 - i\theta_m^2 \cdot \frac{z}{c}\Delta\omega(1+\frac{\Delta\omega}{\omega})} \} \qquad (3.25)$$

When $\Delta\omega = 0$ we of course must obtain the same as in the previous section because the two reflection surfaces then coincide. When $\Delta x = 0$ we have, neglecting phase factors:

$$R(\Delta\omega,z) = \frac{1}{\sqrt{1 - i\theta_m^2 \frac{z}{c}\Delta\omega(1 + \frac{\Delta\omega}{\omega})}}$$

$$\exp\{ - 2(\frac{h_m}{c})^2(1 + 2 \frac{A^2\omega(\omega+\Delta\omega)}{m^2}) \Delta\omega^2 \} \qquad (3.26)$$

To interpret this we note that:

$$A = \omega \cdot \frac{2M\varepsilon_o}{g \cdot e^2} = 2 \cdot \frac{M\varepsilon_o}{(\frac{dN}{dz}) e^2} \cdot \omega = 2 \frac{\omega}{\omega_p^2} \cdot L \qquad (3.27)$$

where we have introduced the plasma frequency ω_p and the length L defined by:

$$L^{-1} = \left|\frac{1}{N} \cdot \frac{dN}{dz}\right| \tag{3.28}$$

At the reflection level the frequency equals the plasma frequency ω_p and A therefore simplifies to:

$$A = 2 \cdot \frac{L}{\omega}$$

Substitution into the exponential term in (3.26) gives:

$$\exp\{ - 2(\frac{h_m}{c})^2(1 + 8 (\frac{L}{m})^2) \Delta\omega^2 \}$$

Because L is the half thickness of the layer and because m is the vertical scale of the irregularities we expect $\frac{L}{m} >> 1$. The half width of the exponential factor now becomes:

$$\Delta\omega_c = \frac{1}{4} \cdot \frac{c}{h_m} \cdot \frac{m}{L} \tag{3.29}$$

which must be compared with the width of the angular spectrum factor which is the same as for a single reflector, see (3.11). The condition for the vertical scale to be detectable becomes $\Delta\omega_c < \Delta\omega_z$ which leads to:

$$z < 4 \cdot \sqrt{3} \cdot \frac{L}{m} \cdot \frac{h_m}{\theta_m^2} = \sqrt{6}\ L \cdot \frac{1}{\theta_m} \cdot \frac{1}{m} \tag{3.30}$$

This result should be compared with (3.13). Since θ_m is of the order 10^{-1} and since the half thickness of the F layer, say, is about half the reflection height it seems quite likely that on this model the frequency correlation technique could provide information in addition to the one provided by spatial correlation, viz. on $(\frac{m}{h_m})$.

Turning now to the case of shallow reflectors we obtain with the same approximations as in the previous section:

$$R(\Delta x,\Delta\omega,z) \simeq \exp\{ i (2 \frac{\omega+\Delta\omega}{c} \Delta z + \frac{\Delta\omega \cdot z}{c}) - 2(\frac{\Delta\omega h_m}{c})^2 \}$$

$$\cdot\{1-(\frac{2h_m}{c})^2\omega(\omega+\Delta\omega) \{1 - \frac{\exp\{-(\frac{\Delta x}{l}) \frac{1}{1-i\theta_m^2 \frac{z}{c} \Delta\omega} - \frac{A^2\Delta\omega^2}{m^2}\}}{\sqrt{1 - i\theta_m^2 \frac{z}{c} \omega}} \}) \quad (3.31)$$

With $\Delta x = 0$ and with phase factors suppressed we obtain:

$$R(\Delta\omega,z) \simeq \exp\{ - 2(\frac{\Delta\omega h_m}{c})^2 \}$$

$$\{1 - (\frac{2h_m}{c})^2\omega(\omega+\Delta\omega) \{1 - \frac{\exp(- \frac{A^2\Delta\omega^2}{m^2})}{\sqrt{1 - i\theta_m^2 \frac{z}{c} \Delta\omega}}\}) \quad (3.32)$$

The first exponential factor is essentially unity, and it is the second part of the expression within the last curly bracket that decides the loss of correlation. The depth to which the correlation falls is again determined by the depth h_m of the reflector. The width is again determined by two competing factors. The half widths of these are:

$$\Delta\omega_c \simeq \frac{\omega}{2} \cdot \frac{m}{L}$$

and

$$\Delta\omega_z \simeq \frac{\sqrt{3}}{\theta_m^2} \cdot \frac{c}{z}$$

The condition for the vertical scale m to be detectable hence becomes:

$$z < \frac{\sqrt{3}}{\pi} \cdot \frac{L}{\theta_m^2} \cdot \frac{\lambda}{m} \quad (3.33)$$

where λ is the free space wavelength. If θ_m is of the order of $\frac{1}{10}$ and the wavelength is not smaller than the vertical scale by more than a factor of about 100 the vertical scale might be detectable.

It should be pointed out here that the models employed so far are of somewhat doubtful validity in that the waves are considered to be travelling as if in free space up to the reflection level. In fact, the wavelengths are increasing toward infinity near the reflection level and it might be that the vertical scale effect on the frequency correlation is largely overestimated by this method.

3.3 Reflection from a plane reflector in a blobby medium

In this and the next subsection we consider the random amplitude and phase variations as imposed on the waves through volume effects and not as above through the reflection from a rough surface. In the present subsection we consider the reflecting surface to be plane and perfectly reflecting and to be embedded in a blobby medium. The vertical distance between the reflection level and the reference level at $z = 0$ is D, and all the scattering blobs are considered to be located between these two levels. We shall limit ourselves to large scale blobs by assuming the horizontal scale to satisfy the inequality:

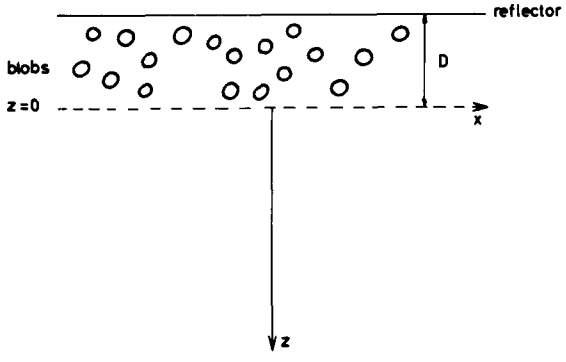

Figure 3.? Reflector in blobby medium

$$l > \sqrt{D \cdot \lambda}$$

where λ is the wavelength. With this condition satisfied diffraction effects within the blobby medium need not be considered and the propagation problem becomes one of geometrical optics. We furthermore consider the irregularities to be so weak that partial reflection and bending of the rays can also be neglected. The properties of the medium are taken to vary in the x and z-directions only, and the medium is irradiated by plane waves along the negative z-axis, as before. When these requirements are met, the random field over the reference plane at $z = 0$ becomes:

$$g(x,\omega,0) = \exp\{ - 2 i \int_0^D K(x,\omega,\eta)\, d\eta \} \qquad (3.34)$$

where $K(x,\omega,z)$ is the complex propagation constant. The real part is related to phase delay and the imaginary part to attenuation. For the unnormalized correlation function at the reference plane we obtain:

$$R'(\Delta x,\Delta\omega,0) =$$

$$\left\langle \exp\{2i \int_0^{D(\omega)} K^*(x,\omega,\eta)d\eta - \int_0^{D(\omega+\Delta\omega)} K(x+\Delta x,\omega+\Delta\omega,\eta)d\eta\}\right\rangle_{av} =$$

$$= \left\langle \exp\{2i(\int_0^{D(\omega)} \triangle K(x,\omega,\eta)d\eta - \Delta\omega \cdot \frac{\partial}{\partial\omega} \int_0^{D(\omega)} K(x,\omega,\eta)d\eta)\}\right\rangle_{av} \qquad (3.35)$$

where we have expanded the exponent to first order in $\Delta\omega$ and where we have put $\Delta K = K^*(x,\omega,z) - K(x+\Delta x,\omega,z)$. It is convenient to separate phase and attenuation effects by putting: $K = k - i\kappa$, which means that

$$\Delta K = (k(x,\omega,z) - k(x+\Delta x,\omega,z)) - i(\kappa(x,\omega,z) + \kappa(x+\Delta x,\omega,z)) =$$

$$= (k - k') - i(\kappa + \kappa') \qquad (3.36)$$

The integral $\int_o^D (k - k')\, d\eta$ is simply the difference in phase delay between two paths separated by a distance Δx. The derivative with respect to frequency of the phase delay is the group travel time T between the levels $z = 0$ and $z = -D$. In the absence of absorption the following simple expression therefore applies:

$$R(\Delta x,\Delta\omega,0) = \left\langle \exp\{ 2i \int_o^D (k - k')d\eta - i\Delta\omega \cdot T \} \right\rangle_{av} \qquad (3.37)$$

To evaluate the space and frequency correlations at the reference plane we have to evaluate the probability distribution of:

$$\alpha = 2 \int_o^D (k - k')d\eta$$

and

$$\beta = 2\left(\frac{\partial}{\partial\omega} \int_o^D k \cdot d\eta - \left\langle \frac{\partial}{\partial\omega} \int_o^D k\, d\eta \right\rangle_{av}\right) \qquad (3.38)$$

The neglect of absorption effects is a good approximation above about 100 km for frequencies higher than about one MHz. For k we use the expression:

$$k = \frac{\omega}{c}\mu = \frac{\omega}{c}\sqrt{1 - X} \qquad (3.39)$$

where $X = \frac{N(x,z)e^2}{M\epsilon_o\omega^2} = \frac{\omega_p^2}{\omega^2}$. Here the electron density $N(x,z)$ consist of two parts:

$$N(x,z) = N_o(z) + \Delta N(x,z) \qquad (3.40)$$

where $\Delta N(x,z)$ is a random deviation from the local mean value. For the random part we make the assumptions:

$$\left\langle \Delta N(x,z) \right\rangle_{av} = 0$$

$$\left\langle \Delta N(x,z)^2 \right\rangle_{av} = N_m^2(z) \tag{3.41}$$

$$\left\langle \Delta N(x+\Delta x, z+\Delta z)\ \Delta N(x,z) \right\rangle_{av} = N_m^2(z) \cdot \exp\{-(\frac{\Delta x}{l})^2 - (\frac{\Delta z}{m})^2\}$$

Because α and β can be considered as a sum of a fairly large number of independent variables they are both gaussian with mean zero and with variances:

$$\left\langle \alpha^2 \right\rangle_{av} = 2\sqrt{\pi}\,(\frac{B}{\omega})^2\, m(1-\exp\{-(\frac{\Delta x}{l})^2\}) \int_o^D \frac{N_m^2(z)}{\mu^2}\, dz \tag{3.42}$$

and

$$\left\langle \beta^2 \right\rangle_{av} = \sqrt{\pi}\,(\frac{B}{\omega})^2\, m \cdot \frac{1}{\omega^2} \int_o^D \frac{N_m^2(z)}{\mu^6}\, dz \tag{3.43}$$

where $B = \frac{e^2}{M\varepsilon_o \cdot c}$. Again we distinguish between deep and shallow phase modulation at the reference plane.

For deep modulation the spatial correlation becomes:

$$R(\Delta x, 0) = \exp\{ - \sqrt{\pi}\,(\frac{B}{\omega})^2\, m \cdot \phi \cdot \frac{1}{l^2}\, \Delta x^2 \} \tag{3.44}$$

where

$$\phi = \int_o^D \frac{N_m^2(z)}{\mu^2}\, dz \tag{3.45}$$

This means that the mean square angular spread becomes:

$$\theta_m^2 = 2\sqrt{\pi}\,(\frac{B}{\omega})^2\,(\frac{c}{l})^2 \cdot \phi \cdot m \tag{3.46}$$

For the frequency correlation at $z = 0$

$$R(\Delta\omega,0) \;=\; \exp\{\, -\sqrt{\pi}\,(\tfrac{B}{\omega})^2\, m \cdot \Psi \cdot (\tfrac{\Delta\omega}{\omega})^2 \,\} \tag{3.47}$$

where:

$$\Psi \;=\; \int_0^D \frac{N_m^{\,2}(z)}{\mu^6}\, dz \tag{3.48}$$

The half width of the corresponding part of the frequency correlation becomes:

$$\Delta\omega_c \;=\; \sqrt{2}\,\frac{1}{\theta_m}\,(\tfrac{c}{l})\sqrt{\tfrac{\Phi}{\Psi}} \tag{3.49}$$

whereas the half width caused by the angular spread is the same as in (3.11). The condition for the vertical scale m to show up therefore requires that:

$$z \;<\; \frac{3}{2}\,\frac{1}{\theta_m}\sqrt{\tfrac{\Psi}{\Phi}} \cdot l \tag{3.50}$$

From this it appears that the horizontal scale l must be large, the opening angle θ_m small and the ratio Ψ/Φ large for the vertical scale m to be observable. If the irregularities are close to the reflection level, Ψ/Φ might become large and make the observation of m possible. However, the model does not appear to be quite satisfactory near the reflection level.

For shallow phase modulation the angular width of the random part of the waves becomes:

$$\theta_m \;=\; \sqrt{2}\;\frac{c}{\omega \cdot l} \tag{3.51}$$

and the condition for the non-angular spectrum part to be the dominant cause of the loss of frequency correlation becomes:

$$z < \sqrt[4]{9\pi}\ \frac{B}{\omega^2} \cdot \frac{c}{\theta_m^2} \cdot \sqrt{m \cdot \Psi} = \sqrt[4]{9\pi}\ \frac{\omega_p^2(z)}{\omega^2} \cdot \frac{1}{\theta_m^2} \cdot \frac{1}{N(z)} \sqrt{m \cdot \Psi} \tag{3.52}$$

Because this inequality depends very strongly on the irregularities near the reflection level through Ψ we shall abstain from any guesses as to the validity of the above inequality.

3.4 Reflection from a linear gradient in electron density with irregularities embedded

The scalar wave equation has recently been solved by a perturbation analysis for weak irregularities embedded in a linear electron density profile (12, 13). The perturbation analysis only holds as long as the perturbation is small in comparison with the unperturbed wave. Putting:

$$g(x,\omega,z) = g_o(x,\omega,z) + g_1(x,\omega,z) \tag{3.53}$$

it is therefore required that $(g_1/g_o) << 1$. This limits the application to cases with shallow fading, or to cases similar to those of shallow phase modulation at the reference level as considered above. As we have seen there is a specular component present in this case. The joint correlation at the observer becomes:

$$\left\langle g^*(x,\omega,z)g(x+\Delta x,\omega+\Delta\omega,z)\right\rangle_{av} = \left\langle g_o^*(x,\omega,z)g_o(x+\Delta x,\omega+\Delta\omega,z)\right\rangle_{av} + \left\langle g_1^*(x,\omega,z)\cdot g_1(x+\Delta x,\omega+\Delta\omega,z)\right\rangle_{av} \tag{3.54}$$

because the average perturbation is zero. The first term does not change in magnitude with $\Delta\omega$ and Δx , but the second one does. It is with the last term we shall be concerned here.

We briefly sketch the evaluation of $g_1(x,\omega,z)$. The scalar wave equation is:

$$\{\nabla^2 + k_o^2(1 + \frac{e^2}{M\varepsilon_o\omega^2} \cdot \frac{N_o}{L} \cdot z) - k_o^2 \frac{e^2}{M\varepsilon_o\omega^2} \Delta N(x,z)\}\, g(x,z) = 0 \qquad (3.55)$$

In this equation all quantities are expanded into Fourier integrals in the x-direction:

$$g_1(x,z) = \int dS \cdot g_1(S,z) \cdot \exp\{ i S k_o x \}$$
$$\Delta N(x,z) = \int dS \cdot \Delta N(S,z) \cdot \exp\{ i S k_o x \} \qquad (3.56)$$

with $k_o = \frac{2\pi}{\lambda}$.

Here λ is the free space wavelength, N_o is the maximum electron density of the layer and L is the semithickness. The situation is illustrated in Figure 3.4. For unit input amplitude of the wave we obtain:

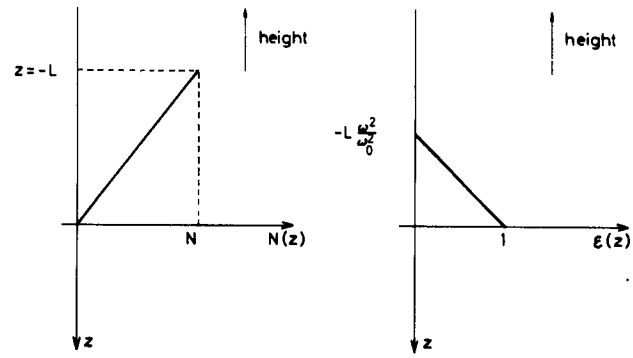

Figure 3.4 Electron density and dielectric constant plotted against z

$$g_1(S,0) = 2\pi(1-S^2)^{-\frac{1}{4}} \frac{\omega^2}{c^2} \cdot \left(\frac{Lc^2}{\omega_o^2}\right)^{\frac{1}{3}} \exp\left\{-i\frac{2}{3}\frac{L\omega^3}{c\omega_o^2}\left((1-S^2)^{\frac{3}{2}} + 1\right)\right\}$$

$$\cdot \int_o^\infty \Delta N(S,-\xi) \cdot Ai\left\{\left(\frac{\omega_o^2}{Lc^2}\right)^{\frac{1}{3}}\left(\xi - L\frac{\omega^2}{\omega_o^2}\right)\right\} Ai\left\{\left(\frac{\omega_o^2}{Lc^2}\right)^{\frac{1}{3}}\left(\xi - L\frac{\omega^2}{\omega_o^2}(1-S^2)\right)\right\} d\xi \qquad (3.57)$$

where ω_o is the plasma frequency at the maximum of the layer where $N(z) = N_o$ and where $Ai(t)$ is the Airy integral defined by (14):

$$Ai(t) = \frac{1}{2\pi i}\int_{C_1} \exp\left\{ tq - \frac{1}{3}q^3 \right\} dq \qquad (3.58)$$

with the path of integration as shown in Figure 3.5.

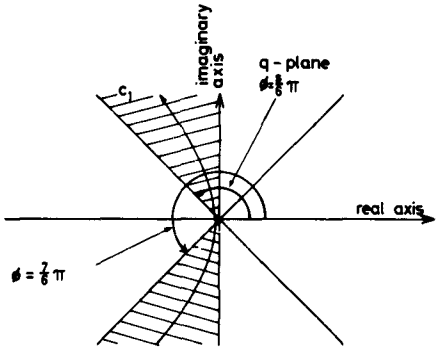

Figure 3.5 Definition of path of integration

The result (3.57) agrees with that of Denisov (12). We first take the inverse transform:

$$g_1(x,0) = \left(\frac{\omega}{c}\right)^3\left(\frac{Lc^2}{\omega_o^2}\right)^{\frac{1}{3}}\int_o^\infty d\xi\ \mathrm{Ai}\left\{\left(\frac{\omega_o^2}{Lc^2}\right)^{\frac{1}{3}}\left(\xi - L\frac{\omega^2}{\omega_o^2}\right)\right\} \cdot$$

$$\cdot \int dS\ \exp\left\{ik_o\left(Sx-\frac{2}{3}L\frac{\omega^2}{\omega_o^2}\left((1-S^2)^{\frac{3}{2}}+1\right)\right)\right\} \cdot \mathrm{Ai}\left\{\left(\frac{\omega_o^2}{Lc^2}\right)^{\frac{1}{3}}\left(\xi-L\frac{\omega^2}{\omega_o^2}(1-S^2)\right)\right\} \cdot$$

$$\cdot \Delta N(S,-\xi) \qquad (3.59)$$

The calculation of the complete joint correlation at the reference level is straight forward but somewhat laborious. We therefore consider only the case of horizontal stratification. With this assumption neglecting phase factors, we obtain:

$$\left\langle g_1^*(x,\omega,0)\ g_1(x,\omega+\Delta\omega,0)\right\rangle_{av} =$$

$$\left(\frac{Lc^2}{\omega_o^2}\right)^{\frac{2}{3}}\left(\frac{\omega}{c}\right)^3\left(\frac{\omega+\Delta\omega}{c}\right)^3\int_o^\infty\int d\xi d\xi' \left\langle \Delta N(-\xi)\Delta N(-\xi')\right\rangle_{av} \cdot$$

$$\cdot \mathrm{Ai}^2\left\{\left(\frac{\omega_o^2}{Lc^2}\right)^{\frac{1}{3}}\left(\xi-L\frac{\omega^2}{\omega_o^2}\right)\right\} \cdot \mathrm{Ai}^2\left\{\left(\frac{\omega_o^2}{Lc^2}\right)^{\frac{1}{3}}\left(\xi' - L\frac{(\omega+\Delta\omega)^2}{\omega_o^2}\right)\right\} \qquad (3.60)$$

If the waves penetrate rather deeply into the layer, i.e. a distance large compared with the vertical scale m, or $m \ll L\frac{\omega^2}{\omega_o^2}$. If this is fullfilled we can introduce the vertical spatial correlation function through:

$$\left\langle \Delta N(-\xi)\Delta N(-\xi')\right\rangle_{av} = \left\langle \Delta N(-\xi)^2\right\rangle_{av} \exp\left\{-\frac{1}{m^2}(\xi-\xi')^2\right\} \qquad (3.61)$$

where the scale m is independent of height. We obtain:

$$\left\langle g_1^*(x,\omega,0)\; g_1(x,\omega+\Delta\omega,0)\right\rangle_{av} =$$

$$\left(\frac{Lc^2}{\omega_o^2}\right)^{\frac{2}{3}}\left(\frac{\omega}{c}\right)^3\left(\frac{\omega+\Delta\omega}{c}\right)^3 \int_o^\infty d\xi \left\langle \Delta N(-\xi)^2\right\rangle_{av} Ai^2\left(\left(\frac{\omega_o^2}{Lc^2}\right)^{\frac{1}{3}}\left(\xi - L\,\frac{\omega^2}{\omega_o^2}\right)\right)$$

$$\cdot \int_{-\infty}^{+\infty} d\eta\; Ai^2\left(\left(\frac{\omega_o^2}{Lc^2}\right)^{\frac{1}{3}}\left(\xi + \eta - L\,\frac{(\omega+\Delta\omega)^2}{\omega_o^2}\right)\right) \exp\{-\eta^2/m^2\} \qquad (3.62)$$

This double integral was evaluated by means of an electronic digital computer for a specific example. We assumed the linear electron density variation to extend over 100 kilometers and the plasma frequency at the peak to be 5 Mc/s. Furthermore, the vertical scale m was allowed to assume the values 0.1 , 0.5 , 1.0 and 10 kilometers. To our surprise the correlation curves are very insensitive to these changes in vertical scale m. This is thought to be caused by the fact that for irregularities at the reflection level these scales are probably all less than the local wavelength, and no pronounced effect of scale change can be expected. The total amount of scattered energy, on

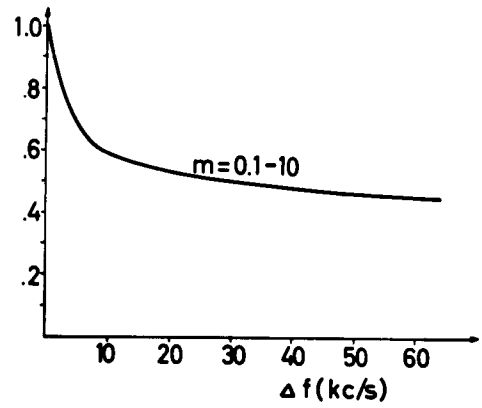

Figure 3.6 Correlation function for horizontally stratified irregularities embedded in a linear electron density profile

the other hand, was very sensitive to scale changes. The total scattered power turns out to be very nearly proportional to the vertical scale m. The correlation curve for the above parameters are shown in Figure 3.5. It is seen to drop very rapidly to about 0.6 over the first 10 kc/s and from there on the rate of decay is very slow. On the basis of this model there does not seem to be much hope for frequency correlation as a method of studying the vertical scale of the irregularities. It must be remembered, however, that the weak scattering approximation on which the analysis is based does break down near the reflection level. For frequency correlation this breakdown might be of comparatively greater importance than for space correlation.

4 CONCLUSIONS

In this report we first studied in rather general terms the properties of waves reflected at two fairly closely spaced frequencies by a random medium. We described the relation between the two reflected waves by means of a correlation function of frequency separation Δw. In the case of an infinitely extended reflector we found that beyond a certain critical distance from the reflector frequency correlation studies can only provide the same type of information as spatial correlation studies. At smaller distances frequency correlation can supply information in addition. For a reflecting medium of limited extent in space we were able to show that frequency correlation tends to a limiting value independent of distance beyond a certain critical distance whereas the spatial correlation range would tend to increase with distance.

When examining several ionospheric models we encountered the same difficulties as are familiar in connection with the interpretation of spatial correlation. For deep phase modulation vertical scale cannot be deduced unambiguously in the same way as with horizontal scale in diversity experiments.

The most important result of the analysis presented above is the suggestion that spatial and frequency correlations should be measured simultaneously in order to prevent angular spectrum effects from being interpreted as arising from irregular electron density distribution along the vertical direction.

References

(1) Booker, H G, J A Ratcliffe, D H Shinn - Phil Trans Roy Soc A 242, 579 (1950)

(2) Briggs, B H, G J Phillips, D H Shinn - Proc Phys Soc B 63, 106 (1950)

(3) Bramley, E N - Proc Instn Elect Engrs, Pt I, 98, 19 (1951)

(4) Hewish, A - Proc Roy Soc A, 209, 81 (1951)

(5) Hewish, A - Proc Roy Soc A, 214, 494 (1952)

(6) Frihagen, J, J Trøim - J Atmos Terr Phys 18, 75 (1960)

(7) Gusev, V D, S F Mirkotan - Radiotekh i Elektr 1, 743 (1956)

(8) Ratcliffe, J A - Repts Progr Phys 19, 188 (1956)

(9) Briggs, B H - Proc Phys Soc 77, 305 (1961)

(10) Hagfors, T - J Geophys Res 66, 777 (1961)

(11) Feinstein, J - Trans I.R.E. AP2, 23 (1954)

(12) Denisov, N G - Izvestiia VUZ, Radiofizika 3, 208 (1960)

(13) Pitteway, M L V - Proc Roy Soc A 254, 86 (1960)

(14) Budden, K G - "Radio Waves in the Ionosphere", Cambridge University Press, (1961) Chapter 15

Part II

OBSERVATIONAL TECHNIQUES AND RESULTS

SUMMARY

The present paper discusses four different methods of studying the correlation between signals reflected from the ionosphere at closely spaced frequencies. These methods are applied to echoes from the F-layer at 4 Mc/s. The correlation width of the random component is found to be highly variable between 10 and 100 kc/s depending on the conditions. Such a frequency correlation range might be explained by the finite opening angle of the angular power spectrum of the reflected waves. A significant specular component is observed in most of the records. Apparent vertical drift velocities as high as 40 m/s are occationally recorded, but more typically velocities of 20 - 25 m/s are found.

1 INTRODUCTION

In the present part of this report we discuss the principles of observation of the correlation between signals reflected from the ionosphere at vertical incidence at slightly different frequencies. The technical details of the equipment used is described in part III of this report. Here we only deal with equipment questions insofar as they are of importance for the interpretation of the experimental data.

The results presented below are only concerned with frequency correlation. Due to the somewhat unexpected signal behaviour described below it did not prove possible to carry out simultaneous spatial and frequency correlation studies within the time available. This is particularly unfortunate in the light of the theoretical discussion of part I and in view of the results obtained below.

In section 2 we state the observational problem arising in the determination of the correlation between the two signals. Several different

techniques to study this relation are then discussed in some detail. In section 3 we present the observational results obtained by means of these techniques, and analyse the results with a view to obtaining information on some of the properties of the reflecting medium. It should be noted that the results thus obtained are so limited that the "typical" behaviour of the ionospheric layers with respect to frequency correlation cannot be established. The reason for this is our inability to pick observational periods at random because of interference problems, absorption effects or violent non-stationary fading. In section 4 we discuss the results obtained by us and by others in the light of the theories developed in part I of this report.

2 METHODS OF OBSERVATION

In the theoretical discussion of part I of this report we considered the signals at the two closely spaced frequencies at the receiver as two random phasors rotating at different angular velocities. This velocity difference is determined by the difference in frequency of the two sidebands transmitted. Suppose that this frequency difference is removed after reception. We are then left with two phasors which are, on the average not rotating in any systematic manner with respect to

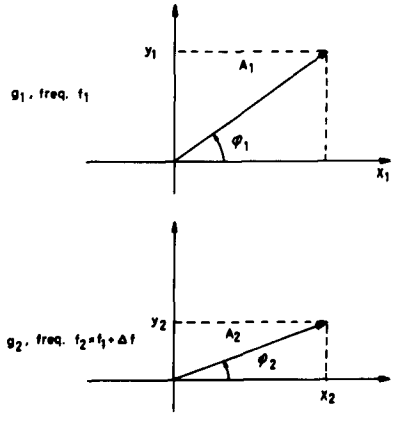

Figure 2.1 Signal phasors at the two frequencies

each other as long as the reflecting medium remains statistically stationary. The two phasors are represented either by their x,y components or by their polar coordinates A,ϕ as shown in Figure 2.1.

The statistical relationship between the two phasors can be described by means of the quantities:

$$\left\langle x_1 x_2 \right\rangle_{av} \quad , \quad \left\langle y_1 y_2 \right\rangle_{av}$$
$$\left\langle x_1 y_2 \right\rangle_{av} \quad , \quad \left\langle x_2 y_1 \right\rangle_{av} \tag{2.1}$$

Because of symmetry we shall assume that:

$$\left\langle x_1 x_2 \right\rangle_{av} = \left\langle y_1 y_2 \right\rangle_{av}$$
and
$$\left\langle x_1 y_2 \right\rangle_{av} = -\left\langle x_2 y_1 \right\rangle_{av} \tag{2.2}$$

In terms of the polar coordinate representation we have:

$$\left.\begin{aligned}
\left\langle x_1 x_2 \right\rangle_{av} &= \tfrac{1}{2}\left\langle A_1 A_2 (\cos(\phi_2-\phi_1) + \cos(\phi_1+\phi_2)) \right\rangle_{av} = \\
&= \tfrac{1}{2}\left\langle A_1 A_2 \cos(\phi_2-\phi_1) \right\rangle_{av} \\
\left\langle y_1 y_2 \right\rangle_{av} &= \tfrac{1}{2}\left\langle A_1 A_2 (\cos(\phi_2-\phi_1) - \cos(\phi_1+\phi_2)) \right\rangle_{av} = \\
&= \tfrac{1}{2}\left\langle A_1 A_2 \cos(\phi_2-\phi_1) \right\rangle_{av} \\
\left\langle x_1 y_2 \right\rangle_{av} &= \tfrac{1}{2}\left\langle A_1 A_2 (\sin(\phi_2-\phi_1) + \sin(\phi_1+\phi_2)) \right\rangle_{av} = \\
&= \tfrac{1}{2}\left\langle A_1 A_2 \sin(\phi_2-\phi_1) \right\rangle_{av} \\
\left\langle x_2 y_1 \right\rangle_{av} &= \tfrac{1}{2}\left\langle +A_1 A_2 (\sin(\phi_1+\phi_2) + \sin(\phi_1-\phi_2)) \right\rangle_{av} = \\
&= -\tfrac{1}{2}\left\langle A_1 A_2 \sin(\phi_2-\phi_1) \right\rangle_{av}
\end{aligned}\right\} \tag{2.3}$$

This is related to the complex representation of part I through:

$$g_1 = \frac{1}{\sqrt{2}} A_1 \exp\{ i \phi_1 \}$$

$$g_2 = \frac{1}{\sqrt{2}} A_2 \exp\{ i \phi_2 \} \qquad (2.4)$$

Using the definition that $\langle g_1^* g_2 \rangle_{av} = R_g$ we find that

$$\langle x_1 x_2 \rangle_{av} = \langle y_1 y_2 \rangle_{av} = \mathrm{Re}(R_g)$$

and (2.5)

$$\langle x_1 y_2 \rangle_{av} = -\langle x_2 y_1 \rangle_{av} = \mathrm{Im}(R_g)$$

In the autocorrelation analysis of a noise signal the two phasors which are correlated are taken from a single signal and the average phase difference of the two phasors is zero. In the case considered here the two phasors are derived from different signals which have been reflected from the ionosphere at different frequencies. This means that a systematic phase difference does exist between the two and that this difference depends strongly on the modulation frequency Δf. This can be seen most easily by means of the following model: Suppose the ionosphere is a plane, perfectly reflecting surface at height H. In this case the phase difference becomes:

$$\phi_2 - \phi_1 = \Delta\phi = \frac{4\pi}{c} H \cdot \Delta f \qquad (2.6)$$

Therefore, even with relatively small large-scale variations in height the two phasors will rotate with respect to each other. This in turn means that the two phasors to be correlated are not related to each other in the same simple way the two phasors occurring in the autocorrelation analysis of gaussian noise. The rate of rotation $\Delta\dot{\phi}$ is related to the apparent vertical velocity through:

$$v = \frac{c}{4\pi} \frac{\Delta\dot{\phi}}{\Delta f} \tag{2.7}$$

Because of this phase uncertainty the distinction between real and imaginary parts of R_g looses its significance, and it is the magnitude $|R_g|$ which really matters.

In the discussion so far we have imagined the random signal to have properties like those of band-pass-limited gaussion noise. As will be shown below there is in many cases a systematic "specular" component present in addition to the random noiselike component described above. Such a specular component could arise through reflection at a shallow phase modulating reflector as we saw in part I of the present report. The presence of such a specular component has important implications on the determination of $|R_g|$ for the random component from post-detection data. The quantity which can be determined directly by the methods described below is the post-detection correlation coefficient defined by:

$$R_A = \frac{\langle G_1 G_2 \rangle_{av} - \langle G_1 \rangle_{av} \langle G_2 \rangle_{av}}{\sqrt{\langle (G_1 - \langle G_1 \rangle_{av})^2 \rangle_{av} \langle (G_2 - \langle G_2 \rangle_{av})^2 \rangle_{av}}} \tag{2.8}$$

and the relationship between the pre- and the postdetection correlation will depend to some extent on the ratio of the power in the "specular" and the random components:

$$\alpha = \frac{P_1 P_2}{\sqrt{\langle A_1^2 \rangle_{av} \langle A_2^2 \rangle_{av}}} \tag{2.9}$$

where P_1 and P_2 are the amplitudes of the specular components at the two frequencies, and A_1 and A_2 those of the random part. G_1 and G_2 are the resultant amplitudes.

Yet another difficulty arises in the correlation of signals at spaced frequencies when a "specular" component is present. The specular components might have arbitrary phase relationships depending on the distance to the reflector as just explained. If the random components do not arise through scattering or reflection at the same distance as the specular components the relative phases of the random and the specular components in the two sidebands might be different and serious difficulties might arise in the determination of the relation between pre- and post-detection correlations. Consider as an example the particular case of the two random components being completely correlated (identical) and much smaller than the "specular" components. When the two "specular" signals are in phase, the post-detection correlation R_A will be unity. When they are 90 or 270° out of phase $R_A = 0$ and when the phase difference is 180° $R_A = -1$. Clearly, there-

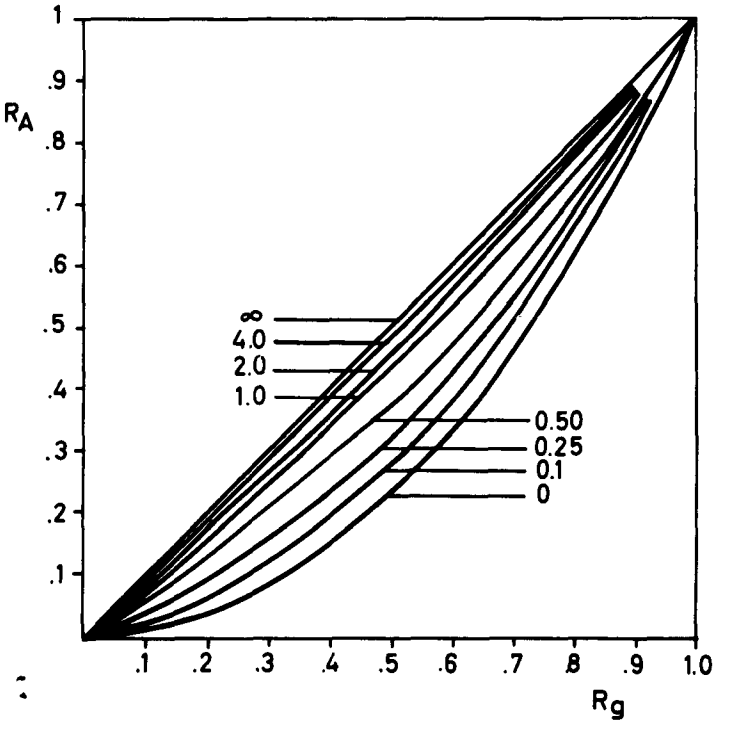

Figure 2.2 Relation between pre- and postdetection correlation for zero phase shift with α = specular/random as parameter

fore, one must be very careful in drawing conclusions about $|R_g|$ from R_A. The relation between $|R_g|$ and R_A has been computed by K Bløtekjær (1) for the case of zero phase difference between specular componehts with α as parameter. The curves are shown in Figure 2.2.

Because of the importance of knowing whether a specular component is present or not the results were checked for a specular component in the following way: In order to compute R_A from our data it was necessary to find $\langle G_1 G_2 \rangle_{av}$, $\langle G_1^2 \rangle_{av}$, $\langle G_2^2 \rangle_{av}$, $\langle G_1 \rangle_{av}$ and $\langle G_2 \rangle_{av}$. From simple application of the theory of gaussian noise with a "specular" component (2) we can find a relation between the quantity

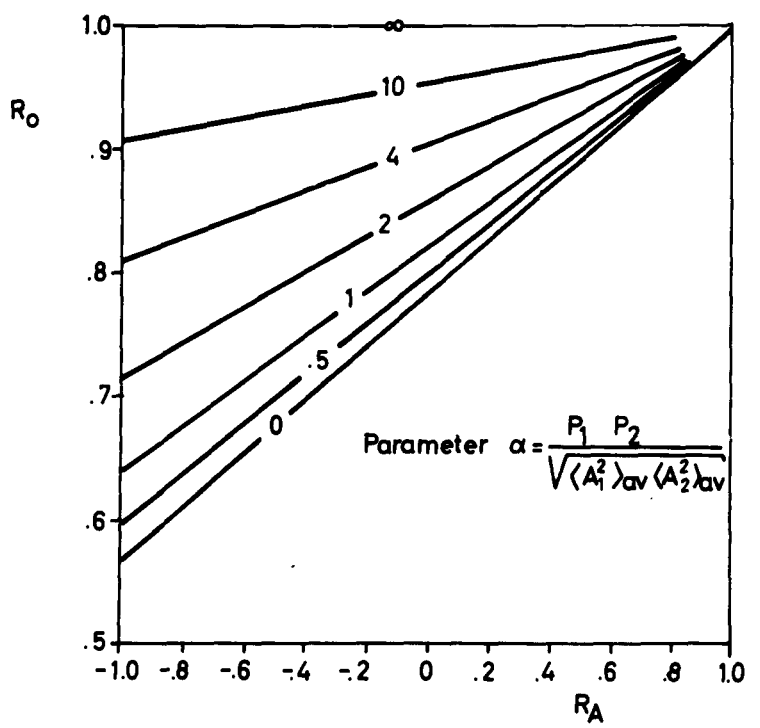

Figure 2.3 Relation between R_o and R_A with α as parameter

$$R_o = \frac{\langle G_1 G_2 \rangle_{av}}{\langle G_1^2 \rangle_{av} \langle G_2^2 \rangle_{av}} \qquad (2.10)$$

and R_A provided $\langle G_1 \rangle_{av} = \langle G_2 \rangle_{av}$ and $\langle G_1^2 \rangle_{av} = \langle G_2^2 \rangle_{av}$. This relation depends on α as defined in (2.9):

$$R_o = R_A + (1-R_A)\,\frac{\pi}{4} \cdot \frac{\exp(-\alpha)}{1+\alpha} \left\{(1+\alpha) I_o\left(\frac{\alpha}{2}\right) + \alpha\, I_1\left(\frac{\alpha}{2}\right)\right\}^2 \qquad (2.11)$$

where I_o and I_1 are Bessel functions with imaginary arguments. This relation is plotted in Figure 2.3 with α as parameter.

2.1 Direct amplitude correlation

The most obvious method to determine the correlation between signals reflected at slightly different frequencies is to correlate their amplitudes directly. As carried out by us the two sidebands were detected

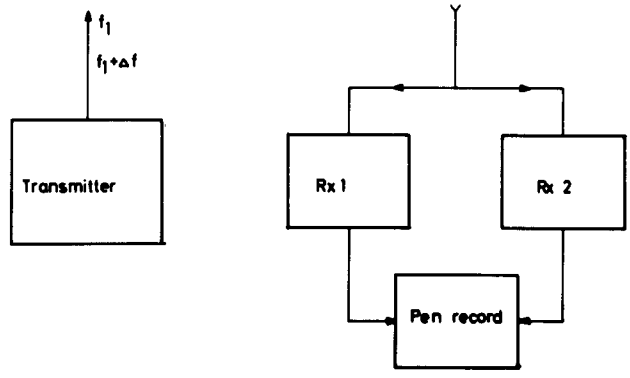

Figure 2.4 Block diagram of direct amplitude correlation

in separate, independent receivers tuned one to each of the sidebands. The detected outputs were fed to a dual channel pen recorder. Correlation coefficients were derived by reading off the amplitude values and correlating the two sets of readings by means of a desk calculator. The system is shown in Figure 2.4. The system works satisfactorily but suffers from the drawback that no phase information is available. When used in connection with calculations by hand the method is quite laborious. Direct amplitude correlation was only used by us in order to check other methods.

2.2 Correlation by sum and difference of signals

Because of the desirability to keep track of the phase relationship of the two sidebands we first tried a method of observation based on principles related to interferometry. On reception of the two sidebands we first removed the systematic frequency difference between the two signals coherently as shown in principle in Figure 2.5. The difference frequency at the transmitter, Δf , is derived from the difference of the frequencies of the two receiver local oscillators LO1 and LO2. The two IF signals were then applied to a circuit shown in Figure 2.6. This circuit forms the sum and the difference of the two signals with zero phase shift and with 90° phase shift applied to one of the signals before adding and subtracting. Further details of the equipment can be found in part III of the report.

By combining the signal phasors g_1 and g_2 as shown in Figure 2.6 we obtain after detection in envelope detectors:

$$\left.\begin{matrix} S \\ D \end{matrix}\right\} = \left(G_1^2 + G_2^2 \pm 2G_1G_2 \cos(\theta_2 - \theta_1)\right)^{\frac{1}{2}} \qquad (2.12a)$$

and

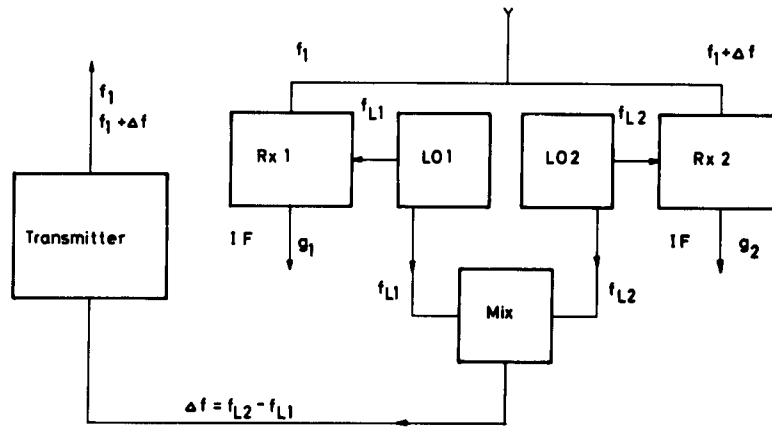

Figure 2.5 Block diagram showing the principle of bringing the two sidebands coherently to the same frequency

$$\left.\begin{matrix}\hat{S}\\ \hat{D}\end{matrix}\right\} = \left(G_1^2 + G_2^2 \pm 2G_1G_2 \sin(\theta_2 - \theta_1)\right)^{\frac{1}{2}} \qquad (2.12b)$$

(We use G and θ here to indicate total signal, possibly consisting

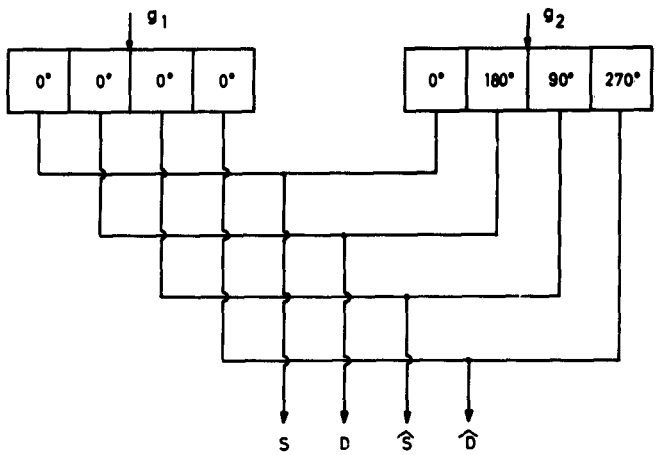

Figure 2.6 Block diagram showing different combinations of the signal phasors g_1 and g_2

of both random and specular components). By adjusting the gain of the receivers or the relative strength of the sidebands transmitted one can make the average values of G_1 and G_2 equal. This means that we can find, by proper averaging the following quantities.

$$\frac{\left\langle G_1 G_2 \cos(\theta_2 - \theta_1) \right\rangle_{av}}{\sqrt{\left\langle G_1^2 \right\rangle_{av} \cdot \left\langle G_2^2 \right\rangle_{av}}} = \frac{\left\langle S^2 - D^2 \right\rangle_{av}}{\left\langle S^2 + D^2 \right\rangle_{av}} \qquad (2.13a)$$

and

$$\frac{\left\langle G_1 G_2 \sin(\theta_2 - \theta_1) \right\rangle_{av}}{\sqrt{\left\langle G_1^2 \right\rangle_{av} \cdot \left\langle G_2^2 \right\rangle_{av}}} = \frac{\left\langle \hat{S}^2 - \hat{D}^2 \right\rangle_{av}}{\left\langle \hat{S}^2 + \hat{D}^2 \right\rangle_{av}} \qquad (2.13b)$$

If the signal were of a gaussian type with no specular component these expressions would give the real and imaginary parts of the complex correlation coefficient R_g. With a "specular" component we would get

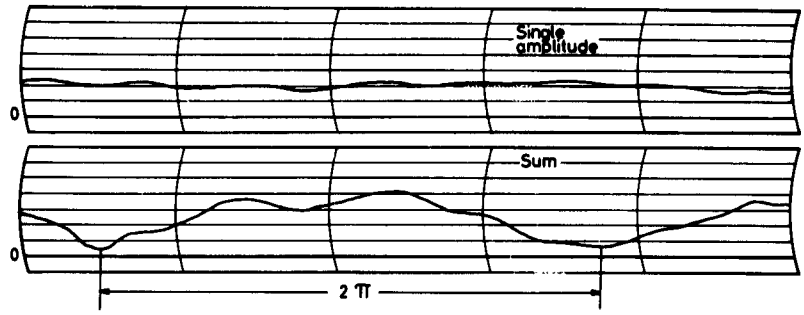

Figure 2.7 Example of a record of S and of the amplitude G of one of the signals

into trouble unless the relative phase of the two "specular" signals were known.

In practice it is not so simple. Due to large scale changes in height the phase of the two phasors will change with respect to each other and we always find that $\langle S^2 \rangle_{av} = \langle D^2 \rangle_{av}$ giving zero correlation. Figure 2.7 shows an example of a record of S and of the amplitude G of one of the signals. We see that the record of G shows very little fading. S on the other hand during the period shown in Figure 2.7 goes through more than one complete fading cycle, which can only be explained in terms of rotation of one of the phasors with respect to the other one. For this particular record as many as 40 complete revolutions were observed during the course of one hour. This record was taken on October 5 1962 at 10-11 hrs. LT at a frequency of 4 Mc/s and with Δf = 31 kc/s. The phase change versus time is shown in Figure 2.8, on the assumption of rotation in the same direction all the time. There is an ambiguity in the direction of rotation in this type of record. Round the points A and B in Figure 2.8 it might be that the direction of rotation reverses. - On the assumption of rotation in the same direction all the time the vertical velocity comes out to be of the order of 25-30 m/s which is rather high, but not impossibly high when compared with observed vertical velocities (3,4). This type of

behaviour was more or less pronounced in all the records made by this method. Because of this phase rotation the evaluation of the magnitude of the correlation coefficient would require the simultaneous recording of $S, D, \hat{S}$ and $\hat{D}$. Due to difficulties in keeping the gain of four channels exactly equal and due to a rather tedious analysing technique, this method was abandoned in the present series of experiments.

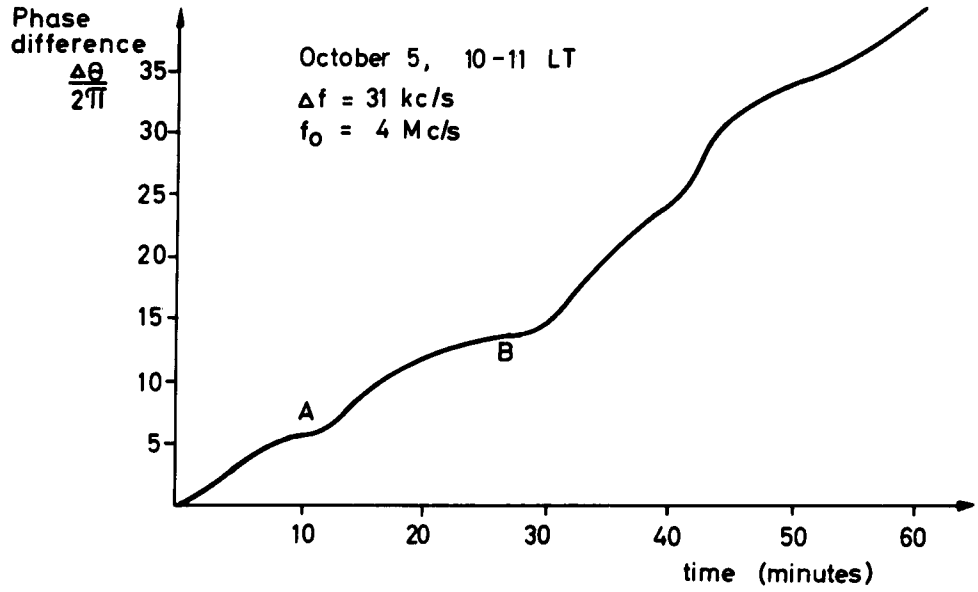

Figure 2.8 Revolution of phasors as a function of time

2.3 Frequency sweep technique

In the expressions (2.12a) or (2.12b) the phase difference $\Delta\theta = \theta_2 - \theta_1$ is determined by the distance to the reflecting medium roughly according to formula (2.6):

$$\Delta\theta = \frac{4\pi}{c} \cdot H \cdot \Delta f$$

For S or D we therefore obtain:

$$\left.\begin{matrix} S \\ \\ D \end{matrix}\right\} = \left(G_1^2 + G_2^2 \pm 2G_1G_2 \cos\left(\frac{4\pi}{c} H \cdot \Delta f\right)\right)^{\frac{1}{2}} \qquad (2.14)$$

Suppose now that we let Δf vary with time, in a linear fashion, say. The result will be that a modulation will be imposed on S and that the depth of this modulation will depend on the product G_1G_2. This incidentally under quiet conditions can be used to determine quite accurately the <u>apparent</u> height of reflection of the signal (h'). Figure 2.9 shows an example of part of such a frequency sweep. The upper channel indicates the frequency difference Δf and the lower channel the sum S. The irregular nature of the record is caused by the manual frequency variation. By counting 26 complete relative revolutions the virtual height was determined to be 228 km at the frequency used, f_o = 4 Mc/s.

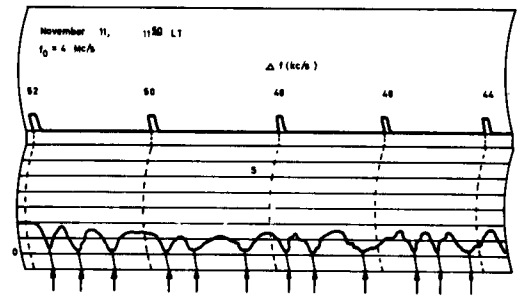

Figure 2.9 <u>Determination of virtual height by frequency change technique</u>

By changing the modulation frequency Δf periodically by about 1500 c/s round some modulation frequency and by noting the values of the maxima and the minima it is possible to determine $G_1 + G_2$ and $|G_1 - G_2|$. By forming the quantity

$$\frac{(G_1 + G_2)^2 - |G_1 - G_2|^2}{(G_1 + G_2)^2 + |G_1 - G_2|^2} = R_o \qquad (2.15)$$

(see (2.10)) the post-detection correlation function can be found from (2.8) by also evaluating

$$\langle G_1 \rangle_{av} = \langle G_2 \rangle_{av} = \tfrac{1}{2} \langle G_1 + G_2 \rangle_{av} \qquad (2.16)$$

This method gives no more information than the direct correlation of individually received signals, but it turns out to be more convenient for manual data reduction because the upper and lower envelopes of the signal modulation can be treated individually. An example of such a record is shown in Figure 2.10. About half of the analysed frequency correlation data were obtained by this technique, see table, Appendix I.

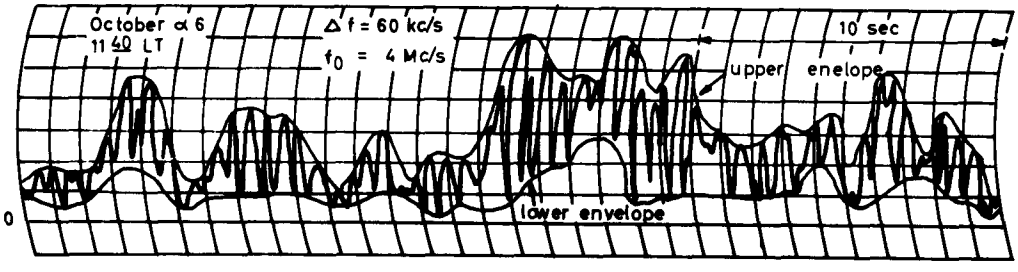

Figure 2.10 Sample of frequency sweep record

2.4 Phase changing technique

The sum and difference technique described in section 2.2 can be modified somewhat as shown in Figure 2.11. The only difference is the addition of a continuous phase changer in one of the signal paths. By

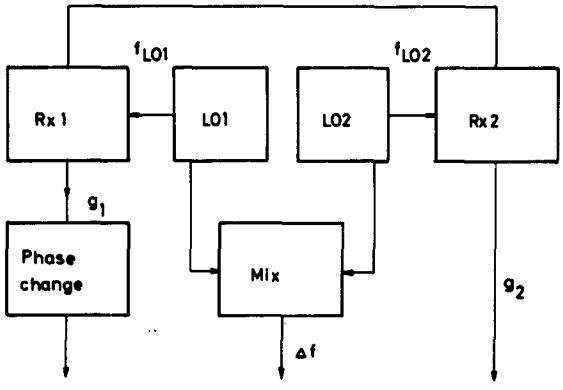

Figure 2.11 Phase changing technique

rotating this phase changer at a constant rate one of the signal phasors can be made to rotate with respect to the other. By recording the sum S as before, it is possible to observe the modulation caused by this rotation, and by reading off the maxima and the minima as in the frequency changing method the amplitude correlation function can be found. An example of such a record is shown in Figure 2.12. On the other channel there are spikes which serve as references to indicate the position of the phase changer. There is one such spike per $\frac{\pi}{2}$ radians of phase change, see Figure 3.4. Phase information can be derived by considering the relative position of the modulation pattern of the signal pattern and the reference spikes. For the analysis of such records we had available an analogue to digital converter and a tape-recorder to store the digital data. The digital data were then analysed in a computer. The following quantities were derived:

$$R_o = \frac{\left\langle S^2_{max} - S^2_{min} \right\rangle_{av}}{\left\langle S^2_{max} + S^2_{min} \right\rangle_{av}} \qquad (2.17)$$

and

$$R_A = \frac{\left\langle S^2_{max} - S^2_{min} \right\rangle_{av} - \left(\left\langle S_{max} \right\rangle_{av} \right)^2}{\left\langle S^2_{max} + S^2_{min} \right\rangle_{av} - \left(\left\langle S_{max} \right\rangle_{av} \right)^2} \qquad (2.18)$$

Furthermore, the relative phase $\Delta\theta$ of the reference spikes and the modulation every ten seconds, and finally an expression for the random phase fluctuations viz.

$$\left\langle \Delta\theta^2 \right\rangle = \frac{1}{n} \sum_{i=1}^{n} \Delta\theta_i^2 \qquad (2.19)$$

This latter quantity is rather difficult to interpret in that it is jointly determined by time variation (time between sampling points about 1 sec) and variation of correlation with frequency.

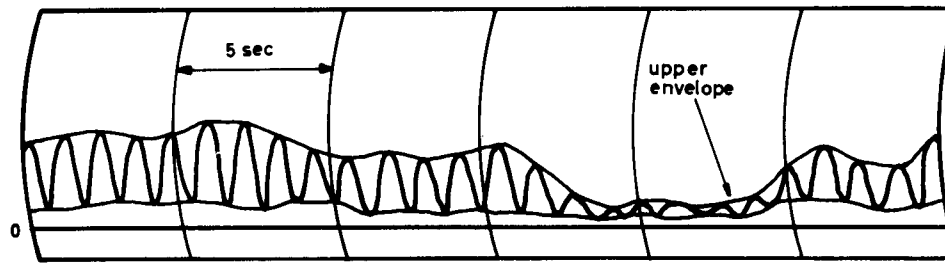

Figure 2.12 Sample from record using phase changing technique

3 OBSERVATIONAL RESULTS

Observations of the correlation between the signal reflected at spaced frequencies at vertical incidence from the ionosphere were begun during September 1962 and continued into the first weeks of January 1963 at Kjeller, near Oslo. All the methods described above except the

straight sum and difference procedure were used for qualitative evaluation of the correlation. In connection with the phase changing method electronic sampling and digital computer analysis was used. Other records were analysed by hand.

The frequency used was 4 Mc/s throughout the experiment, this being the frequency available which was least susceptible to interference. The other two frequencies were 2.7 and 5.4 Mc/s. During the observational period the critical frequency of the F-layer was in the region 5 - 6.5 Mc/s and E-layer frequencies less than 4 Mc/s. Our results - taken during the daytime - therefore pertain to the F-layer. Several attempts were made at observing during the nighttime, but this proved impossible because of severe interference problems. All the results presented below therefore apply for F layer day-time conditions.

For all the successful records the quantities R_o and R_A were calculated as presented in the Table in Appendix I at the end of this part of the report. From R_o and R_A diagrams showing R_o as a function of R_A were plotted for all the records and the strength of the specular component was estimated from a comparison with Figure 2.3. This is discussed in section 3.1 below. Next those data which could be converted into predetection correlation were picked out for special study as described in section 3.2. Finally, in section 3.3, some results from the study of phase variation of the signal are briefly considered.

3.1 Deductions about specular component

Figure 3.1 shows two examples of the evaluation of the ratio of specular power to random power in the returned signal. The lines drawn in full correspond to the best fit with the observational data. Some of the curves of Figure 2.3 are shown dotted in the same diagram. In most of the records a distinct specular component was present and in view of the possibility of the specular components to be out of phase at the two sideband frequencies we did not dare to make any deductions about

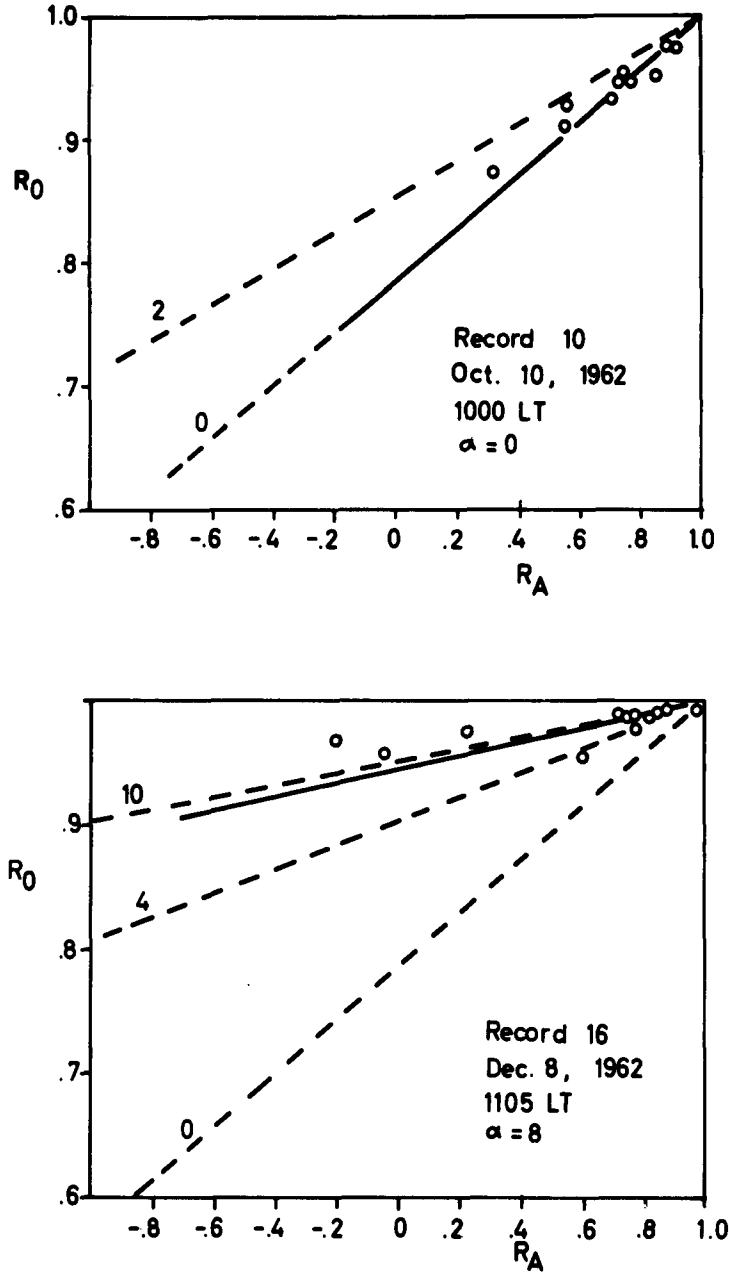

Figure 3.1 Evaluation of specular to random power ratio for records 10 and 16

the predetection correlations for the random component except for very small values of α. From the table in Appendix I it is apparent that the records with phase changing (No 13-20) nearly all have a strong specular component. This is thought to be due to our tendency to make these observations under conditions of fairly slow fading, the reason for this being that the imposed rate of phase rotation should preferably be much higher than the rate of fading of the signal. This was unfortunately only realised after the recordings were completed.

3.2 Correlation coefficients

From the table of records, Appendix I, it is apparent that only the following records can be used for the evaluation of the correlation coefficient of the random reflected component at spaced frequencies: records number 4, 6, 9, 10, 12 and 19. The consistent correlation coefficients from these records were plotted in Figure 3.2. No attempt was made to combine the data into one curve showing correlation against frequency separation because it was realized that condition under which the data were taken could well be as different as is apparent from the observational results. For each of the useful records an attempt was made to draw a curve of correlation versus frequency separation. It was considered sufficiently accurate to draw this curve according to the judgement of the authors rather than according to some least mean square error criterion or the like. There are particularly two points at $\Delta f = 66$ kc/s in record 9 which do not fit the curves at all. Otherwise the points fit the curves quite well. In order to see whether the spread in the data could be explained from statistical errors caused by the finite number of sampling points used in the evaluation of the correlation coefficient we calculated the upper and lower quartiles for the correlation coefficient on the assumptions that a) the two signals correlated originate in a bivariate normal population with correlation coefficient ρ, b) the correlation coefficient ρ is identical with the one shown by the dotted curves in the diagrams and c) that the number of independent pairs of samples giving rise to each

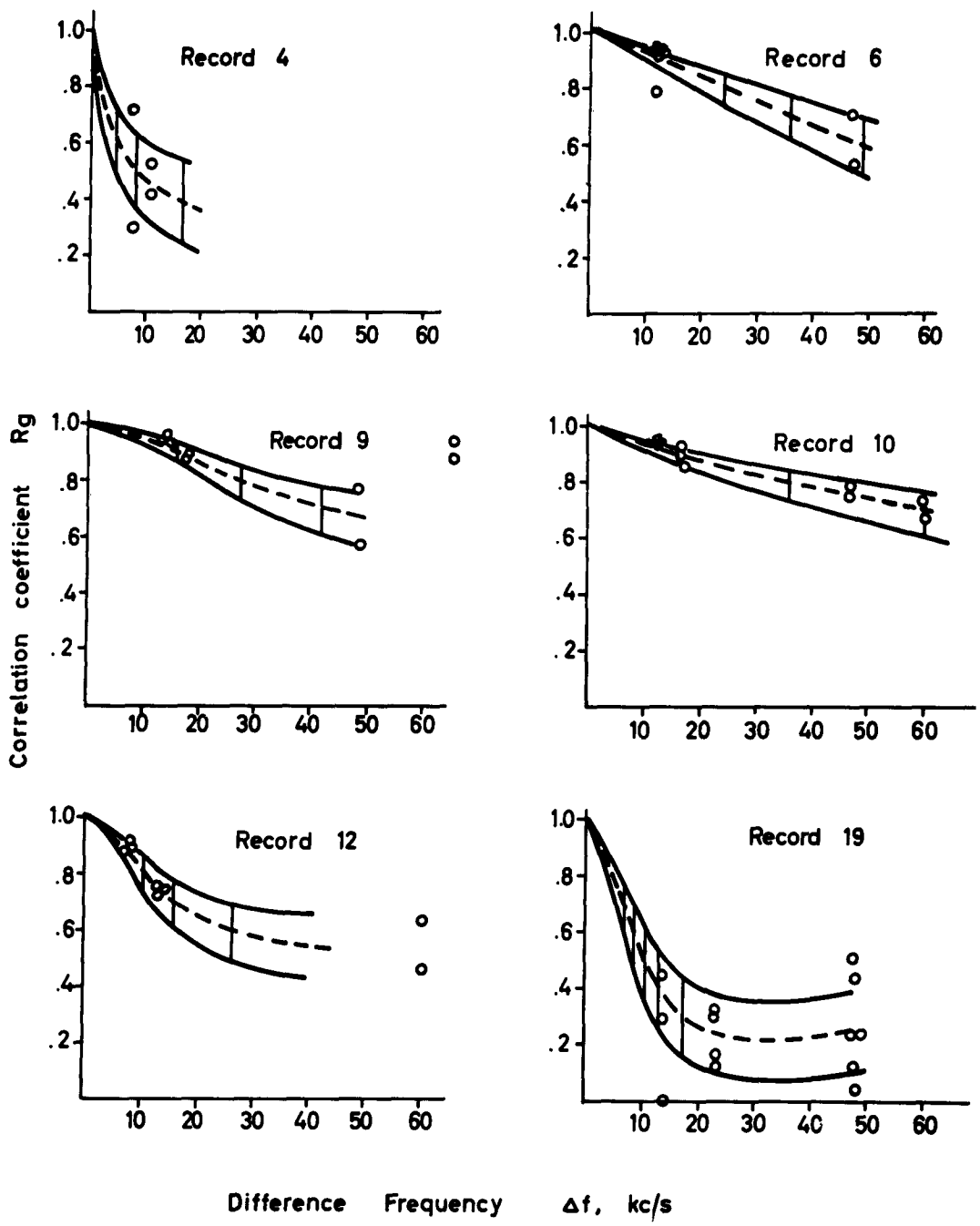

Figure 3.2 Correlation coefficients R_g for various frequency separation Δf for six different records

point in the diagram is 20, which roughly corresponds to the typical number of fading cycles in a record. It is seen that most of the points fall inside this interquartile range. The random spread in the data of the different diagrams can therefore well be explained as purely statistical fluctuations caused by the finite number of sampling points. Details of the evaluation of the interquartile range can be found in Appendix II. The only other source of error which is considered important in the evaluation of correlation coefficients is the possibility of unequal gain in the two channels. As shown in Appendix III this could lead to an error in R_A , ΔR_A given by:

$$\Delta R_A = R_A - R_A' = \frac{\delta^2}{4} \frac{\frac{1}{4-\pi}\{\pi + R_A(8-\pi)\}}{1 + \delta + \frac{8-\pi}{4-\pi} \cdot \frac{\delta^2}{4}} \qquad (3.1)$$

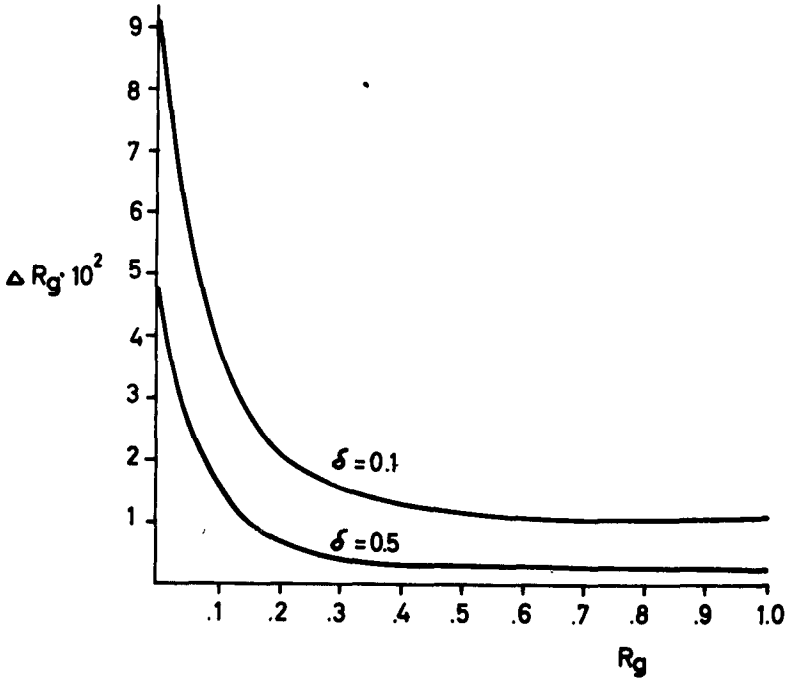

Figure 3.3 Systematic error in R_g due to unequal channel gain

on the assumption of no specular component. Here R_A' is the apparent and R_A the "real" envelope correlation and δ is the excess gain of one of the channels. The corresponding error in the predetection correlation is approximately:

$$\Delta R_g \approx \left(\sqrt{1 + \frac{\Delta R_A}{R_A}} - 1\right) R_g \qquad (3.2)$$

This function is shown in Figure 3.3 for two different values of δ. In our experiment δ is generally smaller than 0.1. The systematic error due to unequal gain is therefore much less than the random errors.

The errors introduced through noise and interference are thought to be unimportant because records were only taken when the signal to noise ratio was good, (better than 10/1 in amplitude). It is therefore concluded that the results in Figure 3.2 represent the real correlation coefficient subject only to the random uncertainties indicated.

3.3 Phase Variation

As explained in section 2.4 the phase changing method should give an opportunity for tracking the phase difference, and the phase was actually printed out for every ten seconds. Upon closer examination of the record it appeared that the phase changes printed out from the sampler-computer combination were rather too large - often leading to apparent vertical velocities of the order of 150 - 200 m/sec. A thorough examination of the record samples revealed that once in a while a sample was missing or an extra sample was inserted due to some sort of spurious noise in the sampling device. This has lead to phase jumps of 90^o here and there in the analysed results. For this reason we have rejected all the phase information in the results analysed automatically. As an example of the type of information which is

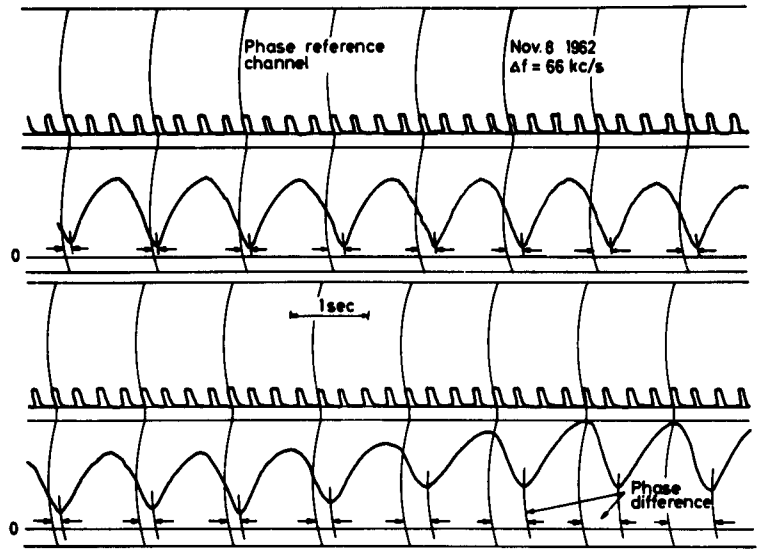

Figure 3.4 Sample from phase changing record showing rapid phase change

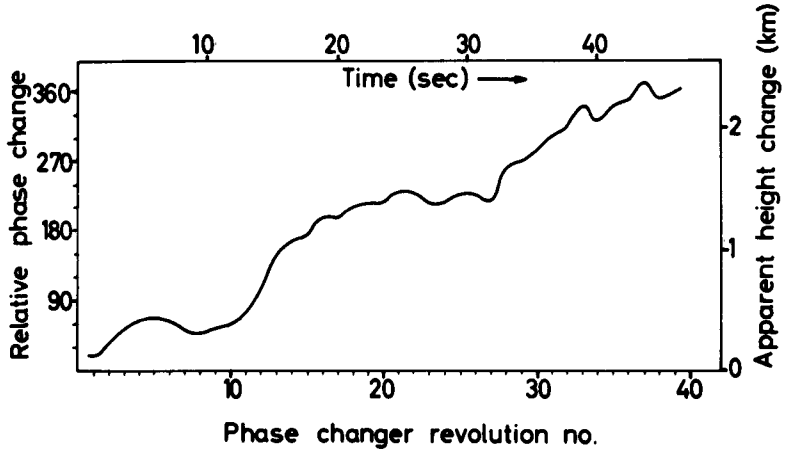

Figure 3.5 Relative phase change versus time deduced from the record shown in Figure 3.4

inherent in the phase changing data we have analysed a few records by hand in order to evaluate possible systematic apparent vertical velocities. An example of a particularly rapid phase variation is shown in Figure 3.4. Part of the corresponding record can be seen in Figure 3.5. The average velocity over the period of this record is 48 m/sec directed upwards. This is exceptionally high. More often we find velocities of the order of 25 m/sec. It is thought that part of the high apparent velocities might be related in some way to the presence of only a few components in the angular spectrum and to an angular flicker of the reflected signal which, in itself quite well could give rise to high apparent vertical velocities over short time intervals. Obviously the simultaneous observation of frequency correlation and direction of arrival would give a very detailed picture of the reflection mechanism.

4 DISCUSSION AND CONCLUSIONS

In the present part of the report we were first able to show that in most of the cases considered here, viz day-time reflections from the F-layer, there is an appreciable specular component present. The presence of this component makes the interpretation of the observations difficult because there might be a different phase relationship between the specular components than between the random component we are interested in.

When no appreciable specular component was present and hence when reliable interpretation of the data could be carried out the correlation appeared to drop to about 0.5 over a frequency separation range somewhere between about 10 kc/s and 100 kc/s. This result appears to be in rather good agreement with the results of Gusev and Mirkotan (3). Before conclusions are drawn about vertical scales the above values should be interpreted in terms of angular spectra of waves as explained in part I of this report. It turns out that the 10 kc/s correlation width can be explained by a θ_m of 23^o and the 100 kc/s by 7.3^o. If, in addition, it is remembered that our theoretical considerations

are based on a one-dimensional analysis, we may conclude that the actually required values of θ_m are even smaller than these because of the two-dimensional nature of the actual reflectors. These values come very close to the θ_m which have been observed by others for waves reflected from the F-layer under similar conditions (4,5). It therefore appears to us that no conclusions about vertical scales should be drawn before simultaneous observations of angular spectrum and frequency correlation can be carried out.

Finally, our observations of the very large fluctuations and changes in the virtual height of reflection of radio waves from the ionosphere probably mean that the ionosphere must be regarded as a large scale deeply corrugated layer with smaller scale irregular structure superimposed.

Acknowledgement

We are indebted to Dr Martin Balser of Lincoln Laboratory for calling our attention to and supplying a copy of the translation of Gusev and Mirkotan's paper (3).

References

(1) Bløtekjær, K - Intern rapport R-86, Norwegian Defence Research Establishment, November (1960)

(2) Rice, S O - Bell Syst Tech J, 24, pp 46-156 Section 4.2 (1945)

(3) Unz, H - J Atmos Terr Phys, 21, 237 (1961)

(4) Woodbridge, D D - J Geophys Res, 67, 4221 (1962)

(5) Gusev, V D
S F Mirkotan - Radiotekh i Elektr 1, 743 (1956)

(6) Bramley, E N - Proc Inst Electr Engrs I, 98, 19 (1951)

(7) Briggs, B H
G J Phillips - Proc Phys Soc B, 106 (1950)

APPENDIX I

Table of records

No	Date	Δf	Duratn	R_o	R_A	α	R_g	Method	Comment
	Sept	16	60	0.72	-0.118		-	Freq sweep	The negative values of R_A are incompatible with α = 0. Not unreasonable large discrepancy between the results of the two methods. Rapid deep fading
	20	16	60	0.705	-0.21		-	" "	
1	0930	16	100	0.786	-0.153	0	-	Direct amp correlation	
		16	100	0.814	0.103		0.33	" " "	
		16	100	0.718	-0.133		-	Freq sweep	
	Sept	11	100	0.972	0.16		-	Freq sweep	With the large specular component the correlation might take on any value depending on the relative phase of the specular signals. No values therefore deduced for R_g. Fading was shallow.
	21	11	100	0.997	0.92		-	Direct amp correlation	
2	1010	11	100	0.915	0.24	8	-	Freq sweep	
		49	100	0.950	0.06		-	" "	
		49	100	0.992	0.71		-	Direct amp correlation	
		49	100	0.948	0.21		-	Freq. sweep	
	Sept	10	100	0.935	0.69		0.74	Freq sweep	Results are somewhat uncertain because of presence of specular component. R_g was deduced assuming zero phase difference between specular components. Medium fading.
	25	10	100	0.962	0.805		0.85	" "	
	1300	10	100	0.947	0.733		0.79	Direct amp correlation	
3		50	100	0.924	0.506	1	0.57	Freq sweep	
		14	100	0.951	0.616		0.67	" "	
		14	100	0.960	0.690		0.74	" "	
		14	100	0.868	0.367		0.43	Direct amp correlation	
	Sept	11	100	0.820	0.263		0.53	Freq sweep	Large fluctuations in correlation coefficients with time. Rapid, deep fading.
	26	11	100	0.776	-0.05		-	" "	
	1345	11	100	0.807	0.164		0.42	Direct amp correlation	
4		8	100	0.863	0.495	0	0.72	Freq sweep	
		8	70	0.778	0.078		0.29	" "	
		8	100	0.846	0.136		0.39	Direct amp correlation	
		17	100	0.790	-0.019		-	Freq sweep	
	Sept	50	100	0.97	0.169			Freq sweep	Too large specular component. Very shallow fading.
5	27	50	100	0.95	0.078	>10		" "	
	1500	70	100	0.95	-0.198			" "	

	Oct	12	100	0.976	0.882		0.95	Freq sweep	Fairly slow but deep fading.
	3	12	100	0.984	0.874		0.94	" "	
	1240	12	100	0.955	0.898		0.95	Direct amp correlation	
		12	80	0.868	0.575		0.77	" " "	
		12	100	0.961	0.802	0	0.91	Freq sweep	
6		12	60	0.949	0.833		0.92	" "	
		47	100	0.716	-0.107		-	" "	
		47	60	0.814	-0.121		-	" "	
		47	100	0.887	0.473		0.70	Direct amp correlation	
		47	100	0.882	0.253		0.52	Freq sweep	
		42	100	0.957	0.015			Freq sweep	A gradual development from slow shallow fading to rapid deep fading as also evidenced by the change in α.
	Oct	42	100	0.944	-0.327	10		" "	
	8	42	100	0.995	0.578			Direct amp correlation	
	1130	60	100	0.953	0.104			Freq sweep	
7		60	100	0.931	0.102			" "	
		60	100	0.985	0.843			Direct amp correlation	
		12	100	0.949	0.622			Freq sweep	
		12	80	0.917	0.443			" "	
		42	100	0.794	0.208		0.47	" "	
		42	100	0.756	0.117	0	0.35	" "	
		42	100	0.802	0.032		0.19	Direct amp correlation	
		16	100	0.954	0.846			Freq sweep	Normal rate comparatively deep fading. Interpretation uncertain.
	Oct	16	100	0.969	0.797			" "	
	10	42	100	0.966	0.618	0		" "	
8	1330	42	100	0.939	0.515	+4		" "	
		66	100	0.971	0.731			" "	
		66	100	0.969	0.885			" "	
		66	100	0.932	0.720			" "	
		66	100	0.824	0.372			Direct amp correlation	

		49	100	0.911	0.568		0.78	Freq sweep	Record exibits normal rate deep fading. Any specular component is small.
	Oct	49	80	0.873	0.308		0.58	" "	
	16	18	100	0.956	0.740		0.87	" "	
	1000	18	100	0.947	0.721		0.86	" "	
9		38	100	0.924	0.587		0.79	" "	
		38	100	0.933	0.721	0	0.86	" "	
		66	100	0.951	0.852		0.93	" "	
		66	100	0.952	0.763		0.89	" "	
		14	100	0.975	0.888		0.95	" "	
		14	100	0.976	0.878		0.94	" "	
		47	100	0.960	0.737		0.79	Freq sweep	The presence of the specular component makes the interpretation uncertain. In view of the systematic behaviour of the correlation coefficient the conversion to R_g was carried out assuming the phase difference of the specular components to be zero.
	Oct	47	90	0.940	0.707		0.76	" "	
	17	17	100	0.967	0.808		0.85	" "	
10	1200	17	100	0.974	0.913		0.93	" "	
		60	100	0.930	0.670	1	0.73	" "	
		60	100	0.940	0.620		0.67	" "	
		13	100	0.987	0.914		0.93	" "	
		13	100	0.986	0.920		0.94	" "	
	Oct	50	100	0.723	-0.12	0		Freq sweep	Rather inconsistant results. R_g not derived.
	18	50	100	0.700	-0.12			" "	
11	1500	50	100	0.944	0.633			" "	
		50	100	0.912	0.345	2		" "	
	Oct	60	100	0.865	0.39		0.65	Freq sweep	Rather deep and rapid fading. Results for larger frequency separations are inconsistent with $\alpha = 0$.
	26	60	100	0.840	0.20		0.47	" "	
	1140	60	52	0.795	-0.21		-	" "	
		42	100	0.725	-0.185		-	" "	
		42	100	0.770	-0.055		-	" "	
12		42	64	0.830	-0.08	0	-	" "	
		13	100	0.910	0.535		0.75	" "	
		13	100	0.910	0.480		0.71	" "	
		13	70	0.920	0.545		0.76	" "	
		86	100	0.950	0.755		0.88	" "	
		86	100	0.960	0.765		0.89	" "	
		86	66	0.960	0.815		0.91	" "	

	Nov	15	60	0.976	0.697		-	Phase changing	Specular component too strong.
13	30	15	60	0.956	0.458	8	-	Machine analysis	
	1225	15	20	0.977	0.507		-	" "	
	Dec	62	60	0.848	0.237		-	Phase changing	Conditions changing rather noticably during record. No interpretation in terms of R_g.
	1	62	60	0.823	0.234		-	Machine analysis	
	1115	62	60	0.817	-0.052	0	-	" "	
		62	60	0.845	0.403	→4	-	" "	
14		52	60	0.981	0.823		-	" "	
		52	60	0.939	0.385		-	" "	
		52	60	0.968	0.823		-	" "	
		52	30	0.956	0.505		-	" "	
		16	60	0.945	0.508		-	" "	
		16	50	0.987	0.958		-	" "	
	Dec	15	60	0.906	0.404		-	Phase changing	Interpretation rather uncertain, again because of specular component. Results are not consistent.
	3	15	60	0.848	-0.079		-	Machine analysis	
	1420	15	50	0.896	0.149		-		
15		43	60	0.910	0.291	1	-		
		43	60	0.879	0.377		-		
		43	20	0.932	0.586		-		
		52	50	0.656	-0.792		-		
	Dec	18	60	0.997	0.972			Phase changing	Interpretation very uncertain. In view of the fairly consistent results it is tempting to assume phase difference of specular components equal to zero and put $R_A = R_g$.
	8	18	60	0.981	0.774			Machine analysis	
	1105	18	60	0.996	0.865				
		18	30	0.994	0.776				
		40	60	0.988	0.761	8			
16		40	60	0.993	0.722				
		40	60	0.993	0.848				
		40	30	0.989	0.823				
		64	60	0.953	0.599				
		64	60	0.965	-0.209				
		64	60	0.957	-0.050				
		64	10	0.974	0.227				

		14	60	0.849	0.008		Phase changing	No interpretation because of sys-
	Jan	14	60	0.943	0.689		Machine analysis	tematic component.
	5	14	60	0.927	0.430			
	1115	14	60	0.976	0.830			
17		47	60	0.918	0.111	3		
		47	60	0.966	0.668			
		47	60	0.953	0.341			
		47	60	0.986	0.877			
		47	60	0.974	0.549			
		47	60	0.923	0.324			
	Jan	16	60	0.992	0.906		Phase changing	No interpretation because of sys-
	5	16	60	0.981	0.822		Machine analysis	tematic component.
	1240	16	60	0.992	0.909			
		16	60	0.994	0.922			
		16	60	0.954	0.543			
18		16	20	0.993	0.918			
		54	60	0.950	0.663			
		54	60	0.914	0.686			
		54	60	0.955	0.586	3		
		54	60	0.934	0.424			
		54	60	0.957	0.691			
		54	60	0.915	0.434			
		64	60	0.988	0.917			
		64	60	0.970	0.821			
		64	60	0.957	0.796			
		64	40	0.945	0.105			

		14	60	0.782	-0.026		-	Phase changing Machine analysis	Interpretation in terms of $\alpha = 0.7$ and phase difference zero. The results appear to be rather inconsistent.
	Jan	14	60	0.831	-0.054		-		
	7	14	60	0.864	0.359		0.45		
	1400	14	60	0.821	0.219		0.29		
		14	60	0.801	0.001		0.00		
		14	50	0.665	-0.261		-		
		23	60	0.809	0.113		0.17		
		23	60	0.820	-0.052		-		
19		23	60	0.849	0.227		0.30		
		23	60	0.840	0.099		0.14		
		23	60	0.833	0.243	0.7	0.32		
		48	60	0.649	-0.360		-		
		48	60	0.785	0.081		0.12		
		48	60	0.886	0.424		0.52		
		48	60	0.829	0.031		0.06		
		48	60	0.715	-0.172		-		
		48	60	0.884	0.174		0.24		
		48	60	0.858	0.376		0.47		
		48	10	0.864	0.177		0.24		
	Jan	9	60	0.757	0.073		0.28	Phase changing Machine analysis	Rapid fading. Some interference toward the end of the recording period. The consistently negative correlation at 17 kHz is not properly explained.
	14	9	60	0.854	0.364		0.63		
	1415	9	60	0.842	0.247		0.52		
		9	60	0.777	0.049		0.23		
20		9	30	0.840	0.348	0	0.61		
		17	60	0.704	-0.204		-		
		17	60	0.681	-0.331		-		
		17	60	0.719	-0.359		-		
		17	60	0.767	-0.330		-		
		17	60	0.651	-0.336		-		
		17	30	0.661	-0.403		-		

APPENDIX II

In order to evaluate the upper and lower quartiles for the correlation coefficient we follow the method described by Fischer (1). We assume that the correlation coefficient R_g is a random variable with mean value ρ. It is furthermore assumed that R_g arises from a finite sample of pairs of values from a bivariate normal distribution with correlation coefficient ρ. According to Fischer the quantity

$$z = \tfrac{1}{2} \ln \frac{1 + R_g}{1 - R_g}$$

is approximately normally distributed about a mean value

$$\langle z \rangle_{av} = \tfrac{1}{2} \ln \frac{1 + \rho}{1 - \rho}$$

with a variance $\frac{1}{n-3}$ where n is the number of pairs of values used for the evaluation of R_g. In our case $n = 20$, and the variance $\mu = 0.0588$. The standard deviation $\sigma = 0.24$. Now, upper and lower quartiles deviate from the mean value by $0.6745\ \sigma = 0.16$. In the following table we give the upper and lower quartiles for a set of different values of the correlation coefficient ρ of the mother populations:

Table A2

ρ	z_{av}	z upper quart	R_g upper quart	z lower quart	R_g lower quart
0.9	1.47	1.63	0.93	1.31	0.86
0.8	1.10	1.26	0.85	0.94	0.74
0.7	0.87	1.03	0.77	0.71	0.61
0.6	0.69	0.85	0.69	0.53	0.49
0.5	0.55	0.71	0.61	0.39	0.37
0.4	0.42	0.58	0.52	0.26	0.25
0.3	0.31	0.47	0.44	0.15	0.15
0.2	0.20	0.36	0.35	0.04	0.04
0.1	0.10	0.26	0.25	-0.06	-0.06

Reference

(1) Fischer, R A - "Statistical Methods for Research Workers". Oliver and Boyd, Edinburgh (1938)

APPENDIX III

Assume that, due to unequal gain in the system, the two observed signal amplitudes a_1 and a_2 are given by

$$a_1 = A_1$$

$$a_2 = A_2(1 + \delta)$$

where

$$\langle A_1 \rangle_{av} = \langle A_2 \rangle_{av} = \langle A \rangle_{av}$$

$$\langle A_1^2 \rangle_{av} = \langle A_2^2 \rangle_{av} = \langle A^2 \rangle_{av}$$

and where δ is the fractional gain difference. If we evaluate the envelope correlation according to (2.18) the apparent envelope correlation becomes:

$$R_A' = \frac{\left\langle (A_1+A_2(1+\delta))^2 - (A_1-A_2(1+\delta))^2 \right\rangle_{av} - \{\langle A_1+A_2(1+\delta) \rangle_{av}\}^2}{\left\langle (A_1+A_2(1+\delta))^2 + (A_1-A_2(1+\delta))^2 \right\rangle_{av} - \{\langle A_1+A_2(1+\delta) \rangle_{av}\}^2} =$$

$$= \frac{R_A(1+\delta) - \frac{\delta^2}{4} \frac{\{\langle A \rangle_{av}\}^2}{\langle A^2 \rangle_{av} - \{\langle A \rangle_{av}\}^2}}{1 + \delta + \frac{\delta^2}{4} \frac{2\langle A^2 \rangle_{av} - \{\langle A \rangle_{av}\}^2}{\langle A^2 \rangle_{av} - \{\langle A \rangle_{av}\}^2}}$$

Using the following expressions for $\langle A^2 \rangle_{av}$ and $\{\langle A \rangle_{av}\}^2$

$$\langle A^2 \rangle_{av} = 2\psi_o$$

$$\{\langle A \rangle_{av}\}^2 = \frac{\pi}{2} \Psi_o$$

and making use of the approximate relation

$$R_A \simeq R_g^2$$

the result (3.1) is obtained.

Part III

DESCRIPTION OF EXPERIMENTAL EQUIPMENT

SUMMARY

A block diagram of the complete experimental equipment is presented and the principle of operation are explained. The equipment is composed of three main parts, and the description of these are given with reference to detailed circuit diagrams. The procedure for adjusting the equipment is briefly described.

1 INTRODUCTION

This part of the report describes the experimental equipment used in the measurement of correlation between radio signals reflected from the ionosphere at adjacent frequencies.

Most of the equipment is of conventional design, and only those features that are specific to the experiment are dealt with in some detail. The description will be given with reference to detailed circuit diagrams and block diagrams that depict the principles of operation.

2 BLOCK DIAGRAM

In this section a brief description of the block diagram of the complete experimental system (Figure 2.1) will be given.

As indicated in the diagram, the equipment is subdivided into three main parts i.e.: the pulse transmitter, the receiver equipment, the detector and recording system.

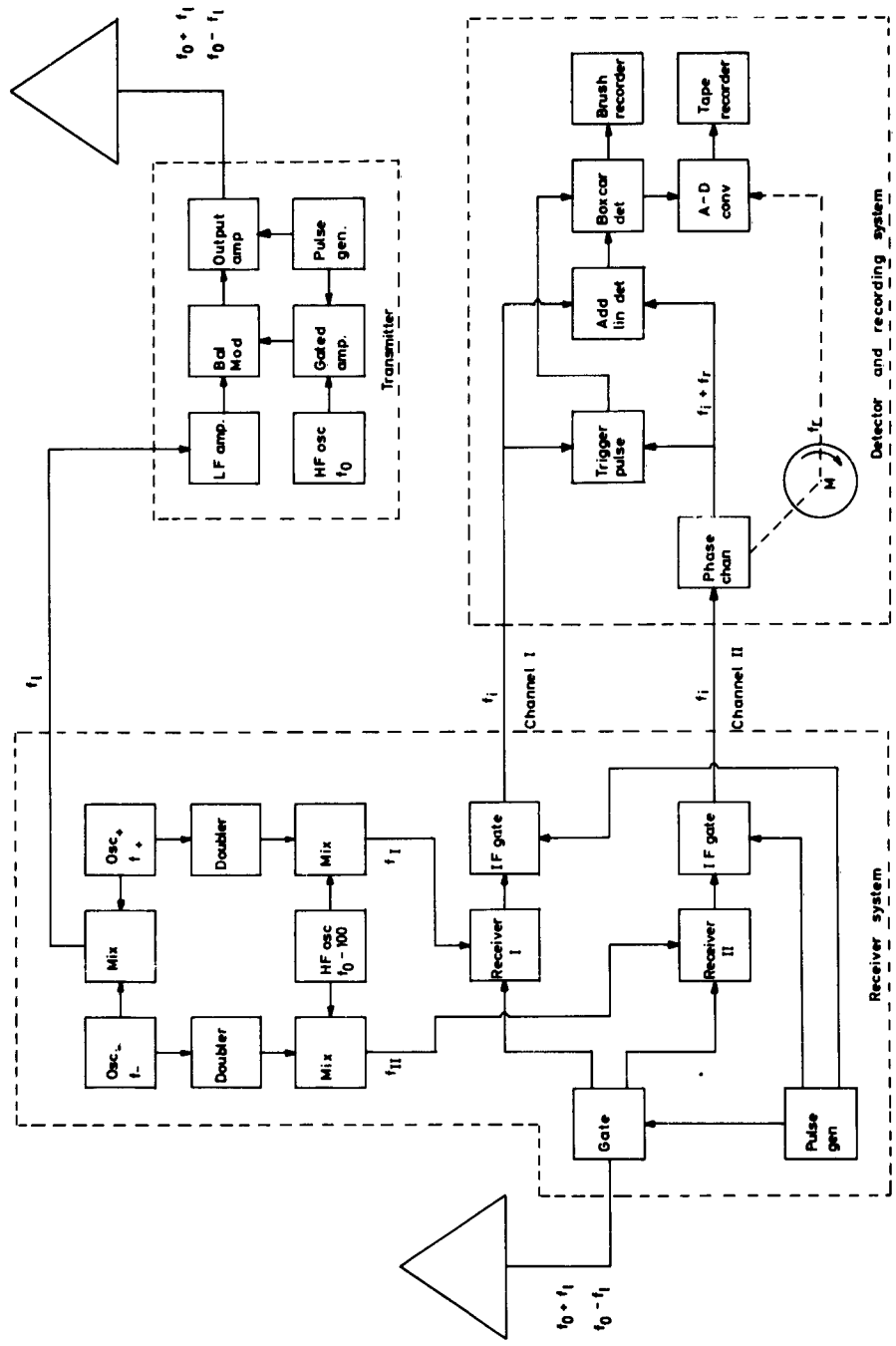

Figure 2.1 Block Diagram of experimental equipment

The pulse transmitter is located in a separate house to shield the receivers from the transmitted pulse. The modulation frequency f_L is sent via cable to the transmitter. The carrier frequency is suppressed and the transmitted pulses therefore contain only two adjacent frequencies $f_o \pm f_L$.

From the receiving aerial the signal passes through a gate to the receivers where the two sidebands present in the echo pulses are separated. To preserve the phase relationship between the two echo signals in the IF channel, the mixer frequencies must be coherent. The subunit on the upper left side of the diagram generates these coherent frequencies and also the modulation frequency f_L. A second gate is inserted into the IF channel. Both this gate and the antenna gate are controlled by the pulse generator, the open period coinciding with the reflected pulse.

In the detector and recording system the signals in the IF channels are combined, detected and finally recorded. To measure the phase between the two signals they are combined with different phase relationships by the phase changer and the addition circuit. The detected video pulses are passed to a box car detector, which is a special sort of peak voltmeter. This peak detected signal is recorded, in analog form on a Brush recorder and in digital form on a tape recorder equipped with an analog-digital converter.

3 DESCRIPTION OF THE PULSE TRANSMITTER

This section describes the pulse transmitter and its auxillary amplifiers with reference to three circuit diagrams (Diagrams 3.1 - 3.3). The aerial system is also described.

3.1 Block diagram

Figure 3.1 gives a more detailed block diagram of the pulse transmitter. The carrier is generated in a crystal oscillator and fed to a balanced modulator through a gated amplifier. The modulator output is amplified in two stages buffer and power amplifier. The latter is gated with the same pulsed signal as the HF-amplifier.

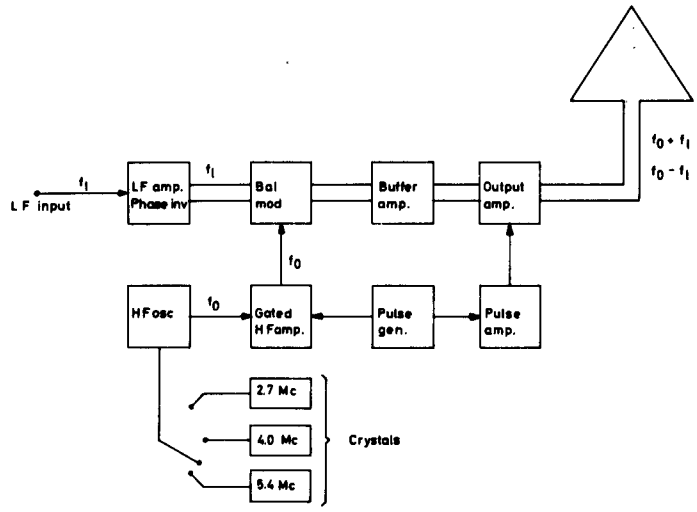

Figure 3.1 Block diagram of pulse transmitter

3.2 HF oscillator

The HF oscillator (Diagram 3.1) can generate three fixed frequencies. It is a type of electron coupled oscillator with crystals as the frequency sensitive elements. The HF signal is amplified in one stage and the output is taken from a cathode follower.

3.3 Pulse generator

A monostable multivibrator is triggered from the A C mains (50 c/s) with adjustable phase. (Diagram 3.1). The pulse duration is variable between 0.5 and 4 msec. The output pulses are amplified and brought out via a cathode follower.

3.4 LF amplifier and phase inverter

The input to the LF amplifier (Diagram 3.2, upper left side) is the modulation frequency f_L. A long tailed pair coupling is used for amplification and phase splitting.

3.5 HF amplifier

This amplifier (Diagram 3.2) consists of a long tailed pair which is gated by current gating to the cathodes. The output is taken through a transformer to prevent the gating pulse from reaching the modulator. The output circuit is heavily damped to obtain a good step response.

3.6 Balanced modulator

The balanced modulator (Diagram 3.2) consists of two valves. The carrier is applied to the control grids with equal phases and the modulating signal to the screen grids with opposite phases. The anode load is centertapped and transformer coupled to the next stage.

3.7 Buffer and power amplifier

These are linear push-pull amplifiers operated in class B. (Diagram 3.2). The tuned circuits are heavily damped to obtain steep pulse

edges. The power amplifier has a maximum output of 800 W unmodulated signal pulses i.e. 400 W modulated signal pulses. It is gated at the grids to achieve good carrier suppression between pulses and to reduce anode dissipation. In Figure 3.2 the shape and frequency spectrum of the transmitted pulse are depicted.

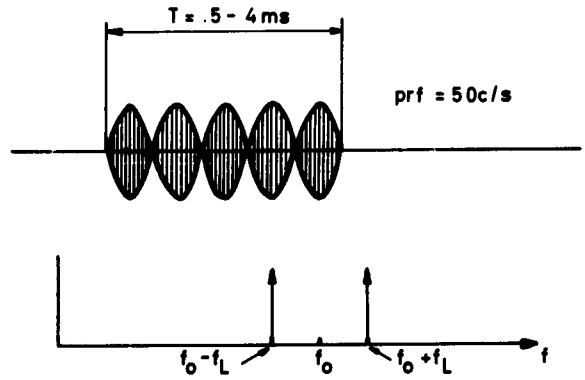

Figure 3.2 Transmitted pulse

3.8 Pulse amplifier

Before being applied to the power amplifier the gating pulse passes through a pulse amplifier (Diagram 3.2). Here the pulse is amplified and clamped by diodes to appropriate levels and fed via a cathode follower to the midtap of the power amplifier grid transformer.

3.9 Power supply

Two stabilized power supplies give plus and minus 300 V with very little ripple. (Diagram 3.3). The plus 600 V source to the power valve screens is only capacitor filtered as is also the 4 kV anode

power supply, since these voltages only need to be approximately constant during the 5 msec pulses which are synchronized to the AC mains.

The high tension supply is variable with an auto transformer. A time relay delays the high voltages allowing for a warm up time of 1 min for the tubes.

3.10 Aerials

Separate transmitting and receiving vertical delta aerials are used, each terminated in a 1100 ohm load. The two aerials are connected to the same 28 m high vertical pole, but mounted at right angles to each other to minimize coupling.

4 DESCRIPTION OF THE RECEIVER EQUIPMENT

This section describes the receiver stage, i.e. the conversion of the faint HF signal from the antenna to two separate, amplified IF signals. The description will be given with reference to seven circuit diagrams (Diagrams 4.1 - 4.7).

4.1 Antenna gate

To prevent the transmitted pulse from reaching the receivers directly a gate (Diagram 4.1) is inserted between the antenna and the receivers. The signal path is opened by a negative pulse from the pulse generator. During the negative pulse the two series diodes will be conducting, whereas the shunt diode is closed. In the interval between pulses only the shunt diode will be conducting, and the signal path is blocked. When the gating pulse coincides with the reflected pulse, only this signal will reach the receivers.

4.2 Pulse generator

The pulse generator (Diagram 4.2) can be triggered either from the AC mains or from an external tone generator of p r f in the range 50-200 c/s. The monostable multivibrator generates positive pulses which are amplified and phase inverted. The phase of the output pulses with respect to the trigger voltage can be chosen arbitrarily, and by means of a potentiometer the pulse width can be varied from 0.4 - 4 msec.

The negative pulses are fed to three separate cathode followers, one supplying pulses to the antenna gate and the two others supplying pulses to the IF gates.

4.3 LF generator

The LF generator (Diagram 4.3) consists of two oscillators and a mixer valve. The two tuning capacitors are mechanically coupled, and the output voltages from the oscillators are of frequency $f_+ = 275$ Kc/s + $f_L/2$ and $f_- = 275$ Kc/s - $f_L/2$ respectively. Care has been taken in design and construction to avoid any interaction between the two separate oscillators. After amplification the two signals are combined in the mixer valve, and in the output the difference frequency f_L appears. By a filter the LF signal is extracted and fed to a cathode follower. The output voltage can be varied by means of a potentiometer.

4.4 HF oscillator

The frequency of the HF oscillator (Diagram 4.4) can be varied in the range 2.5 - 6 Mc/s. The oscillator valve is followed by a tuned amplifier that also provides isolation between the oscillator and the external load.

4.5 External local oscillator system

This system (Diagram 4.5) generates the two mixer signals that substitute the signals from the local oscillator in the receivers. The two voltages are coherent and of frequencies $f_I = f_o + f_L + 450$ kc/s and $f_{II} = f_o - f_L + 450$ kc/s respectively where 450 kc/s is the frequency in the IF channel. The main advantage of this system comes from the fact that the oscillators need not have a high frequency stability. A small relative shift in one or more of the generated frequencies does not affect the operation of the complete system.

The frequency f_I is generated by the following process. The signal of frequency f_+ is fed via a cathode follower (Diagram 4.3) to a triode pentode performing doubling and mixing with the HF signal of frequency $f_o - 100$ kc/s. After successive filtering and amplification the output voltage will be of the sum frequency
$f_I = (f_o - 100) + 2\cdot(275 + f_L/2) = f_o + f_L + 450$ kc/s

Originally the frequency f_I was generated according to the equation $f_I = f_o + 2\cdot(225 + f_L/2)$. This scheme failed because the output from the mixer in addition to the desired signal contained weak signals of frequency $f_I \pm 450$ kc/s giving rise to false signals from the receiver.

4.6 Receiver with output cathode follower

The receivers used were the Eddystone Communication Receiver, Model 680 X. Some minor modifications were necessary to incorporate the receivers in the complete system; (Diagram 4.6).

1) The local oscillator valve was removed and replaced by a connection to the external local oscillator system.

2) As the desired output from the receiver is the IF signal, a cathode follower was mounted into the receiver casing.

3) The receiver was provided with better shielding and aerial connections to prevent any pick up of the transmitted pulse.

4.7 IF gate

To achieve extinction of the signal coming directly from the transmitter it was necessary to have an extra gate in the signal path. This gate was located just after the receiver (Diagram 4.6). The operation is almost identical to that of the antenna gate. The resonant circuit in the connection to the pulse generator provides a large isolation impedance to the IF signal, but negligible impedance to the pulses.

4.8 Mains filter

A mains filter (Diagram 4.7) was used to prevent pick up transmitter signals from reaching the receiver. The filter was inserted in the AC mains line to the receiving equipment.

5 DESCRIPTION OF THE DETECTOR AND RECORDING SYSTEM

This section describes the processing of the IF signals from the receivers. Although many other more elaborate schemes are possible, an advantage of the system used is simplicity and ease of operation. The system is described with reference to five circuit diagrams. (Diagrams 5.1 - 5.4).

5.1 The phase changer

In order to add the two IF signals with different phase relationships, one of the signals is sent through the phase changer (Diagram 5.1). The principle of this device can best be explained in connection with Figure 5.1.

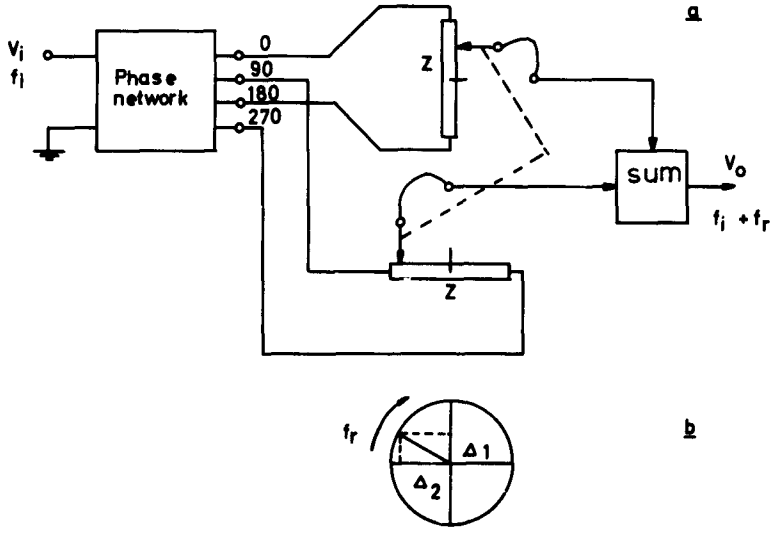

Figure 5.1 Principle of phase changer

Each of the four output voltages from the phase network are of the same amplitude and frequency as the input V_i, but have been shifted in phase as indicated. The two voltages applied across the impedances Z are thus in phase quadrature. As the impedance per unit length is constant, the signal picked up by the sliding contact is proportional to the distance Δ from the mid point.

The movements of the contacts are coupled in such a way that the two deviations Δ_1 and Δ_2 are also in phase quadrature (see Figure 5.1 b). The output voltage V_o will then be identical to the input voltage except for a phase difference θ that is determined by the positions of the sliding contacts. When the mechanical movement corresponds to a uniform rotation f_r in Figure 5.1 b , the phase θ will be a linear function of time. The effect on the output signal is thus equivalent to shifting the frequency slightly by an amount $f_r = d\theta/dt$.

The details of the phase changer are given in Diagram 5.1. The input signal is amplified and transformer coupled to a phase network consisting entirely of resistors and capacitors. The operation of this phase network is independent of frequency in the vicinity of f_i. By means of potentiometers the amplitudes and phases of the output signals can be given the proper values.

The impedance Z is a capacitor consisting of an inner cylinder and an outer cylinder divided into two parts electrically insulated from each other. The inner cylinder is free to move and is equivalent to the pick up contact in Figure 5.1. The two inner cylinders are coupled and driven back and forth by an electro motor, the device very much resembling a steam engine.

The signal currents from the pick up cylinders are added and amplified in a tuned amplifier with variable gain.

5.2 Addition circuit and linear detector

The two echo signals are combined and detected in the circuit shown in Diagram 5.2. The summation is performed by an amplifier with large negative feedback. To reproduce the envelope of the pulses properly, the time constant τ of the detector must satisfy: $1/f_i << \tau << T$,

where T is the pulse width. Due to the phase changer the amplitude of the video output pulses will be oscillating with period f_r.

5.3 Box car detector

The box car detector (Diagram 5.3) is a peak voltmeter with very small time constant for both charging and discharging when working on pulse signals. On the other hand, the time constant in the interval between pulses is approximately infinite. This behaviour of the peak voltmeter is very important when the input signal is varying rapidly.

The desired characteristics are obtained by replacing the usual discharging resistor in a normal single diode rectifier with a valve. This is biased beyond cutoff between pulses, while it is fully conducting when the signal pulses are arriving. In Figure 5.2 the waveforms in the box car detector are shown.

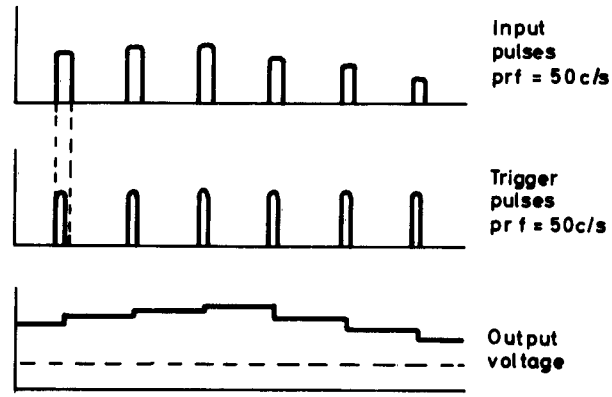

Figure 5.2 Principle of box car detector

To achieve proper operation of the box car detector, the trigger pulses should have a minimum height and be of somewhat shorter duration than the echo pulses as indicated in the figure. The output signal is then the envelope of the input superimposed on a DC-voltage.

5.4 Trigger pulse circuit

The trigger pulses are generated from the echo signals in the nonlinear circuit shown in Diagram 5.4. By successive amplification, detection, clipping and shaping, the output pulses are rendered almost independent of the characteristics of the echo pulses.

The signals in the two IF channels are amplified and detected separately. After addition the video pulses are again amplified and then finally clipped and shaped. Depending on the amplitude of the echo pulses, the valves in the circuit will operate as linear amplifiers (small signals) or limiters (large signals).

The magnitude of the pulses are governed by the two resistors in the voltage divider. The width and shape of the trigger pulse are to a certain extent determined by the components in the pulse shaper.

5.5 Power supply

The power supply serving the detector and recording system is shown in Diagram 5.5. It provides a stabilized voltage at 300 V plus.

5.6 Brush recording equipment

The recorder used is a two channel Brush recorder Type BL202 equipped with a DC preamplifier. The speed of the paper chart is normally

5 mm/s , but in some cases a higher speed has been used. The recording on paper chart is used mainly for adjusting and supervisory purpose. Figure 3.4, Part II shows a sample of a typical recording.

The signal is recorded in the lower channel, whereas each mark in the upper channel corresponds to a sample taken by the A-D converter.

5.7 Analog-digital converter and tape recorder

It is possible to extract the desired information from the recording on paper chart, and in the first phase of the experiment this was actually done. But the manual analysis of even a few minutes registration is very tedious, and facilities for recording on digital form were therefore added to the equipment. The A-D converter and tape recorder are parts of a data processing system developed at NDRE.

The sampling times are controlled by the electro motor that drives the phase changer. As is seen from Figure 3.4, Part II, four samples are taken per revolution of the phase changer. Four protruding knobs spaced 90° apart on a wheel trigger the sampling process. Each sampled value is converted to a nine bit number and finally recorded on magnetic tape.

6 ADJUSTING OF EQUIPMENT

When measurements are made some care must be exercised to obtain proper operation of the equipment and these will be mentioned briefly.

It is desirable to have a transmitted pulse of long duration, and the pulse width should consequently be close to the maximum set by the height of reflection. Furthermore the balanced modulator in the transmitter should be adjusted to get complete suppression of the carrier.

The simultaneous tuning of the receivers is straightforward, but care must be taken to provide equal gain in the two IF channels. This is easy to adjust when the transmitted pulses are received directly (with sufficient attenuation). Due to the phase changer the recorded signal will be oscillating, the minimum being zero when the gains are equal.

It is essential that only the wanted pulses pass through the gates, as any other signals will currupt the operation of the box car detector. The position and width of the gating pulses must therefore be adjusted carefully.

After adjusting the equipment according to these rules the measurements proper are very easy to perform, and there is no need for frequent readjustments.

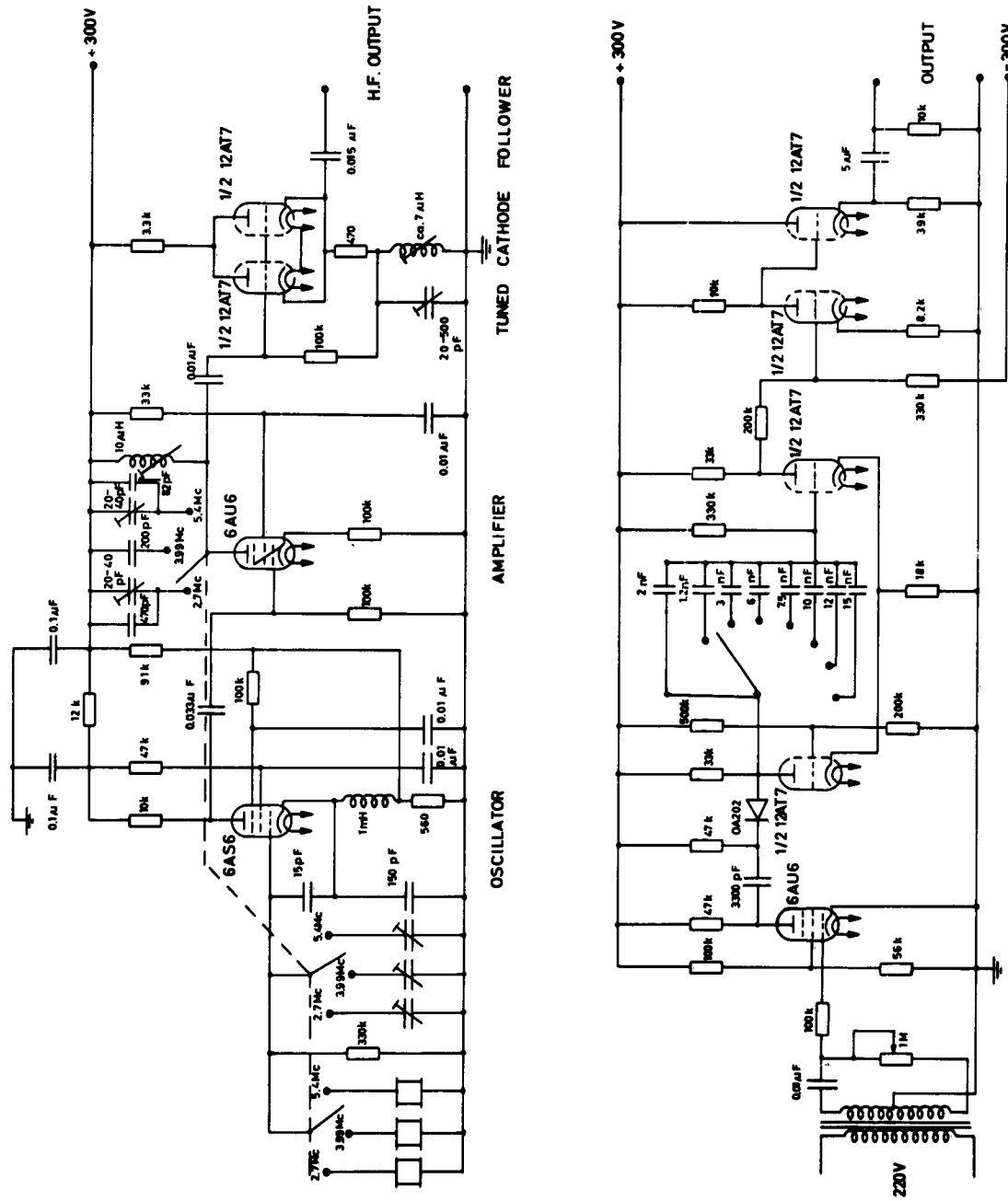

Diagram 3.1 HF oscillator and pulse generator

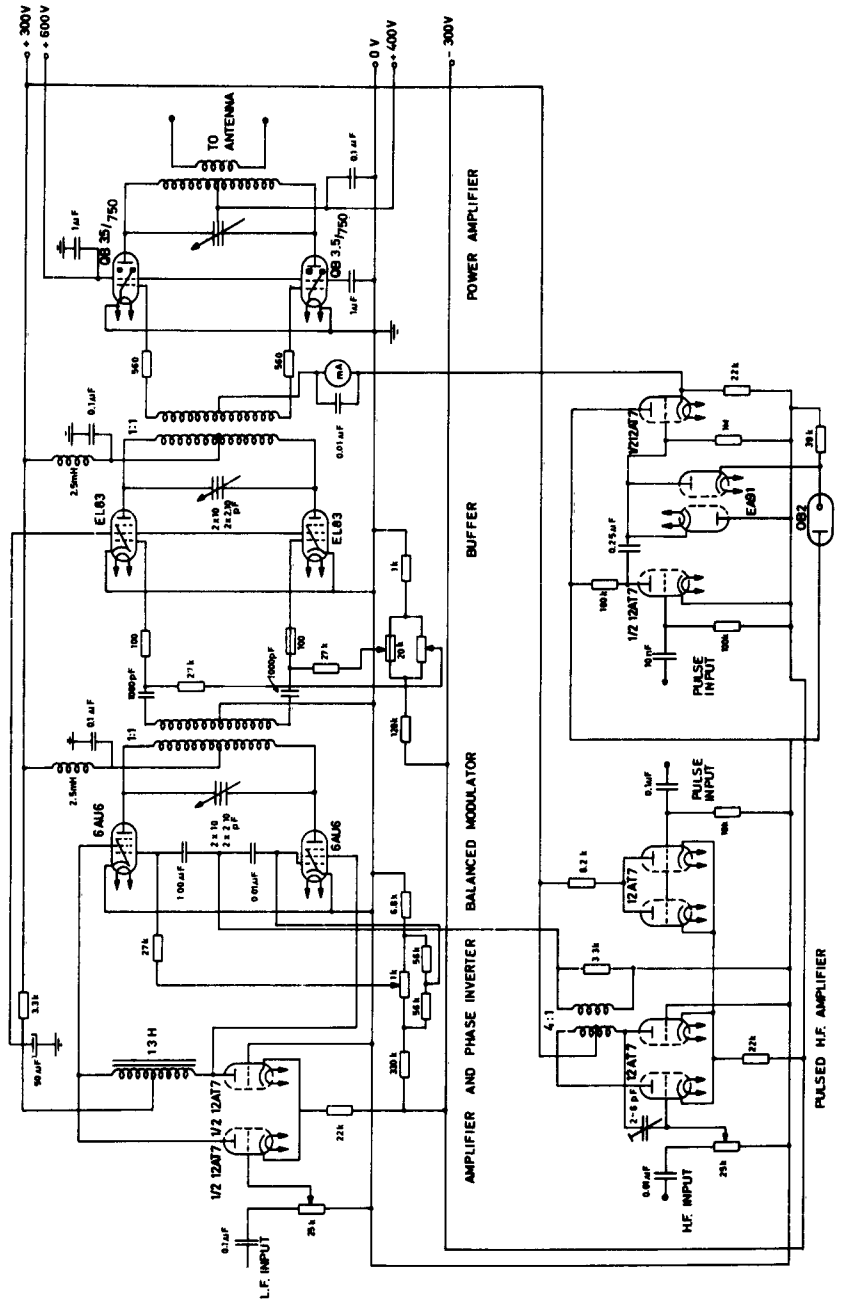

Diagram 3.2 Transmitter

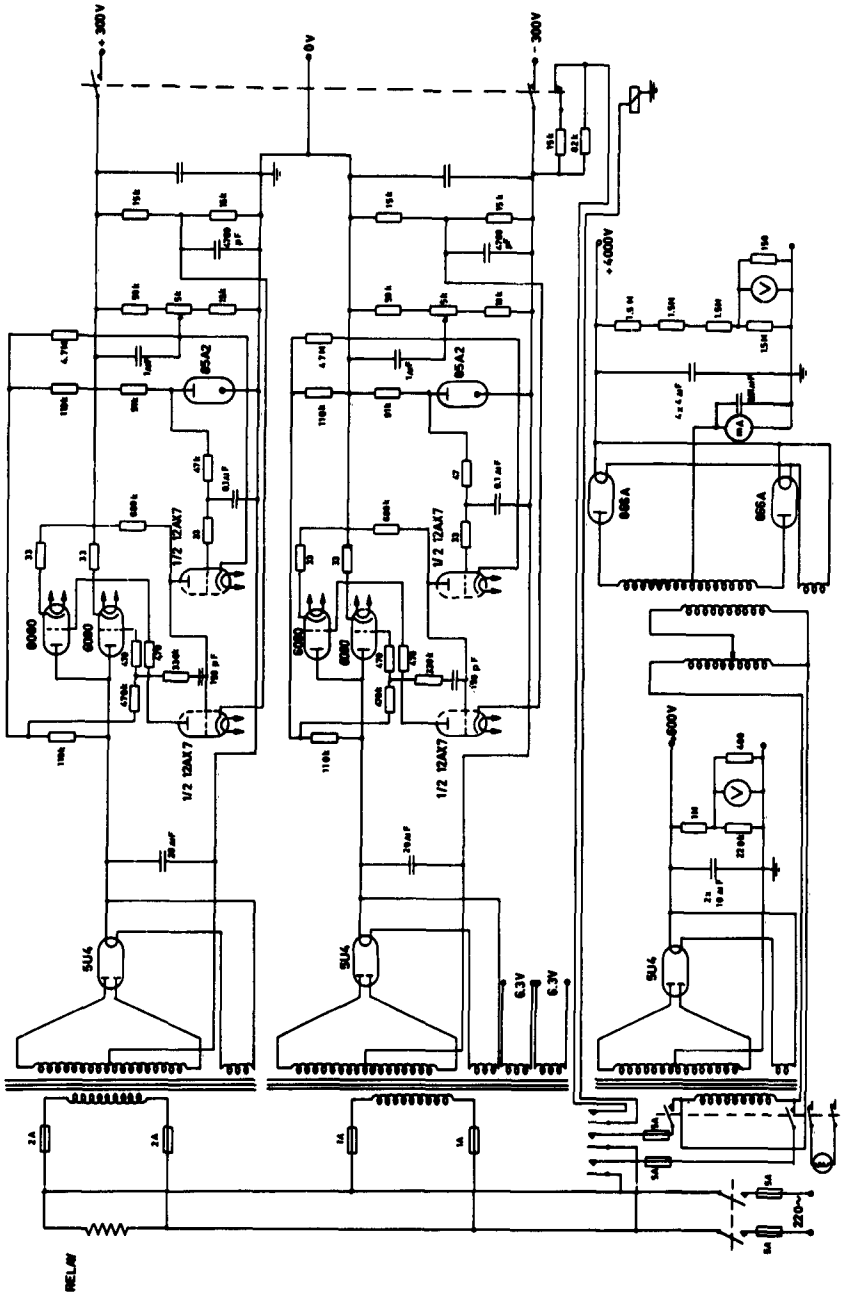

Diagram 3.3 Power supply and voltage stabilizer

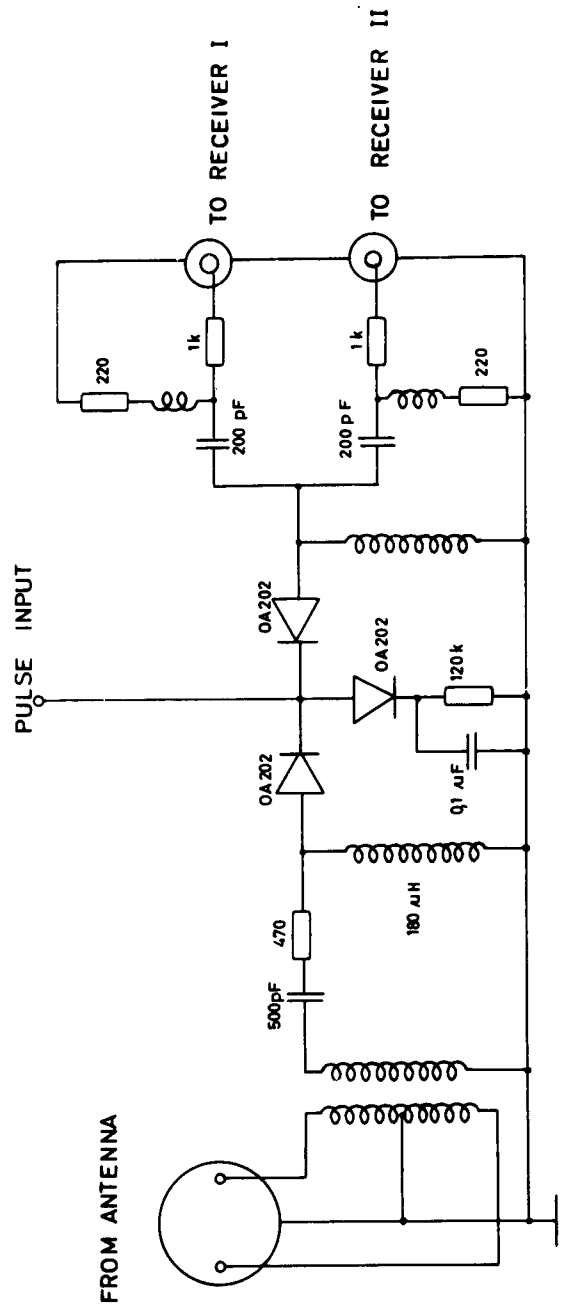

Diagram 4.1 Antenna gate

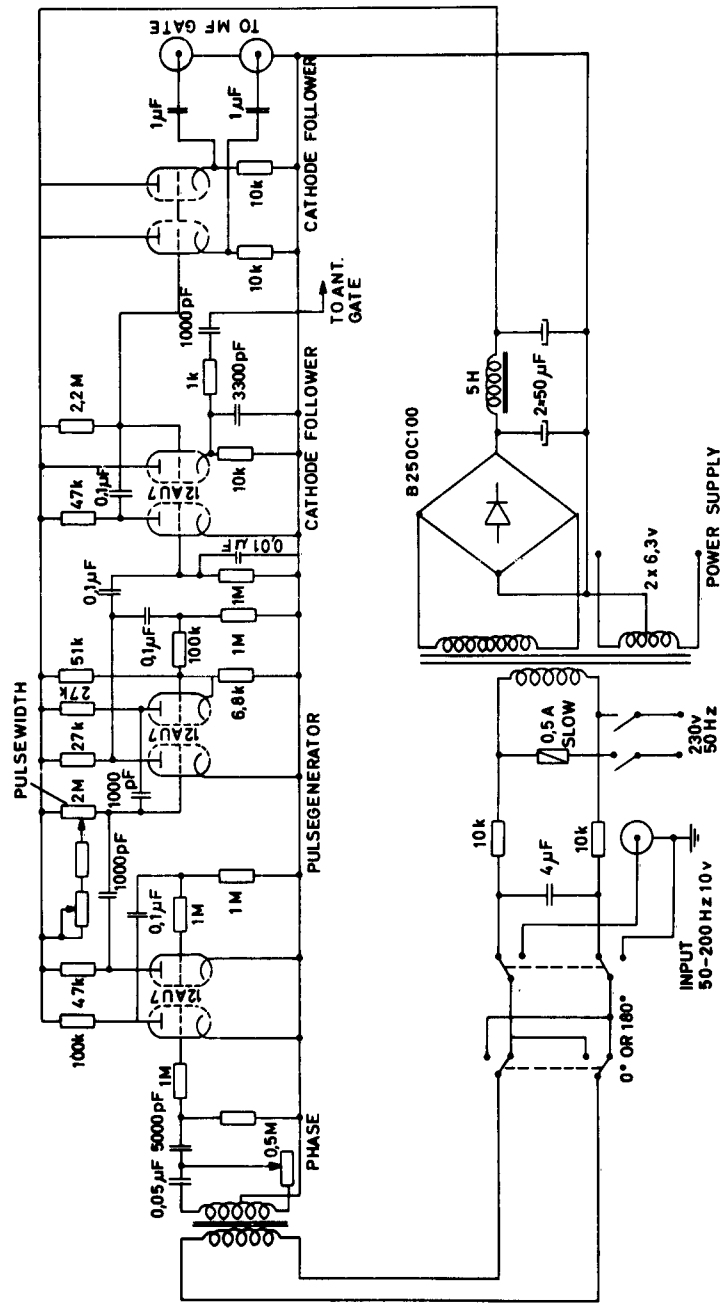

Diagram 4.2 Pulse generator

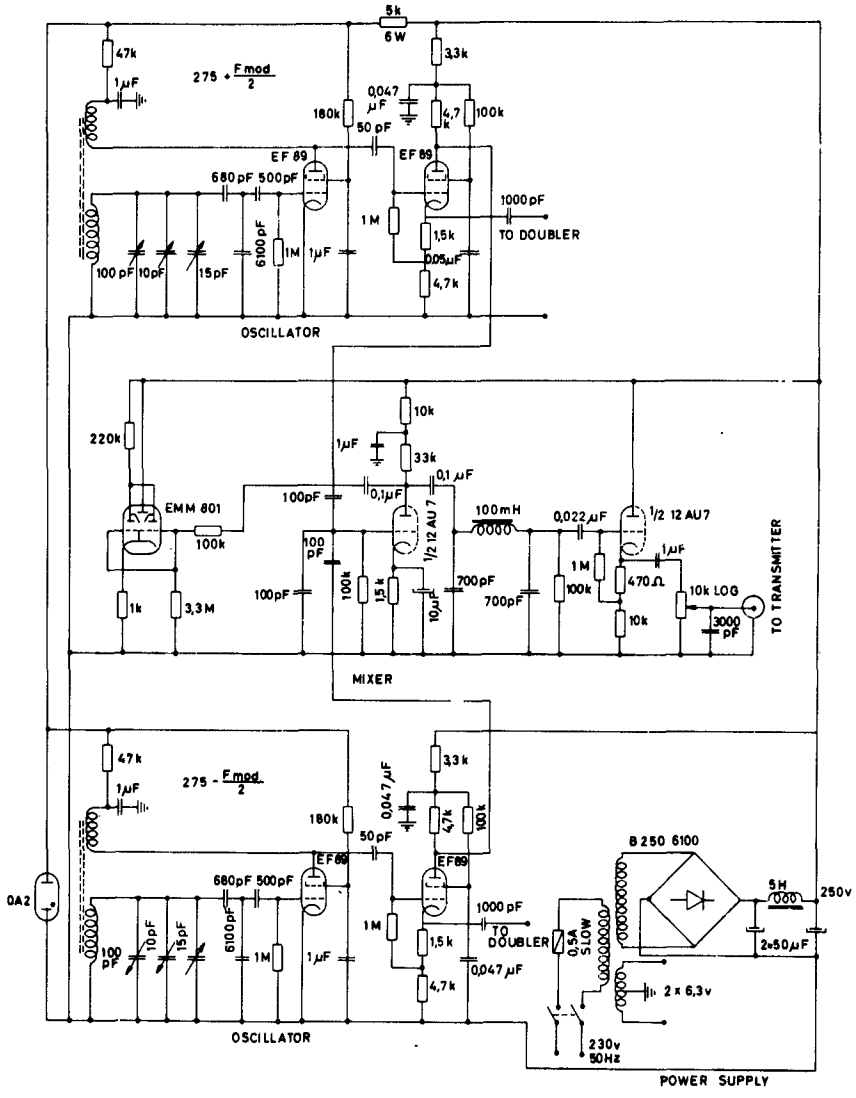

Diagram 4.3 LF generator

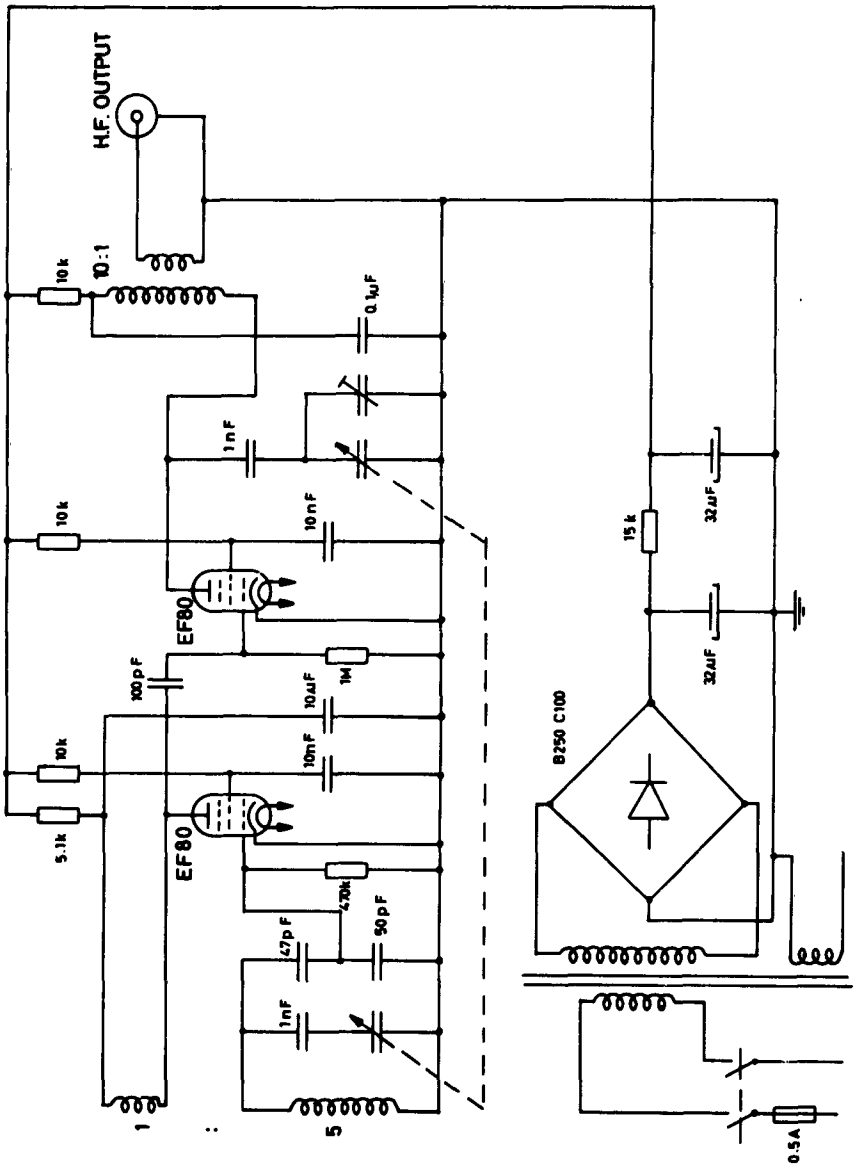

Diagram 4.4 HF oscillator

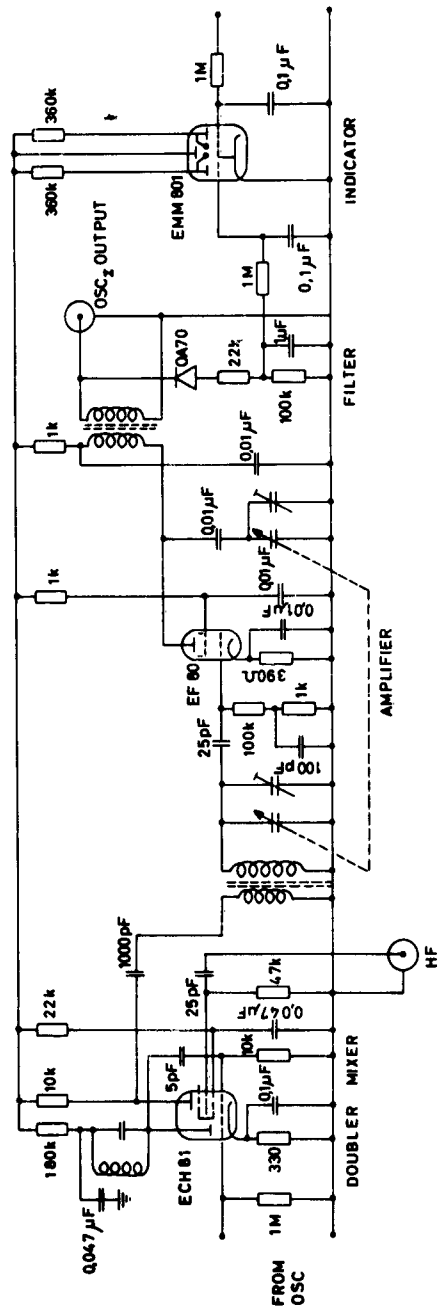

Diagram 4.5 Generator for local oscillator frequency

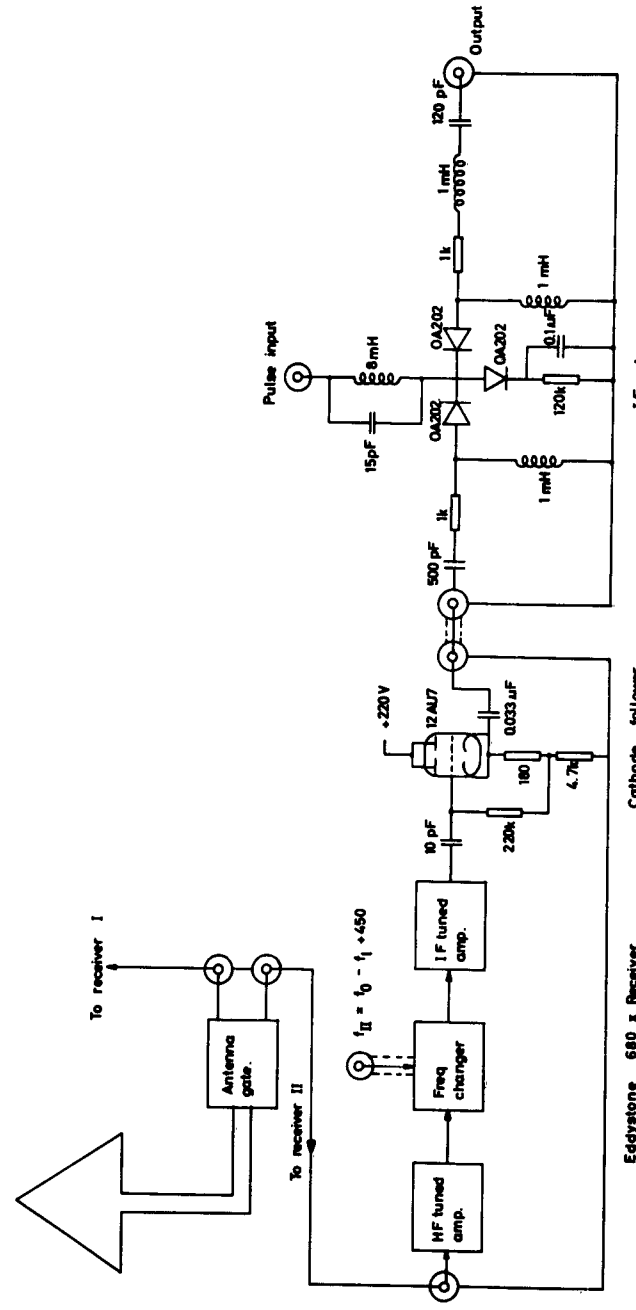

Diagram 4.6 Receiver stage and IF gate

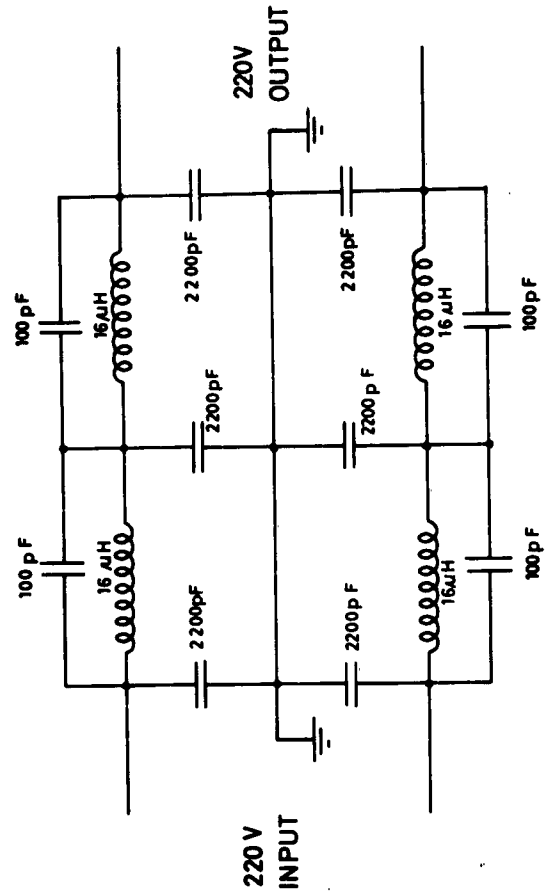

Diagram 4.7 Mains filter

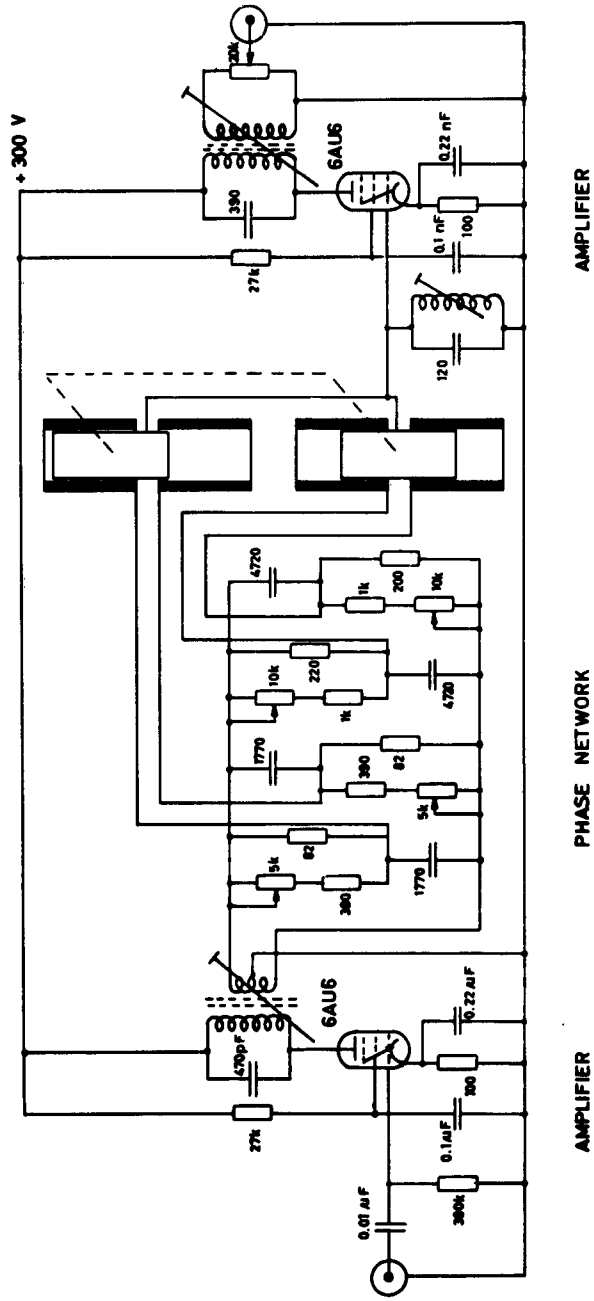

Diagram 5.1 Phase changer

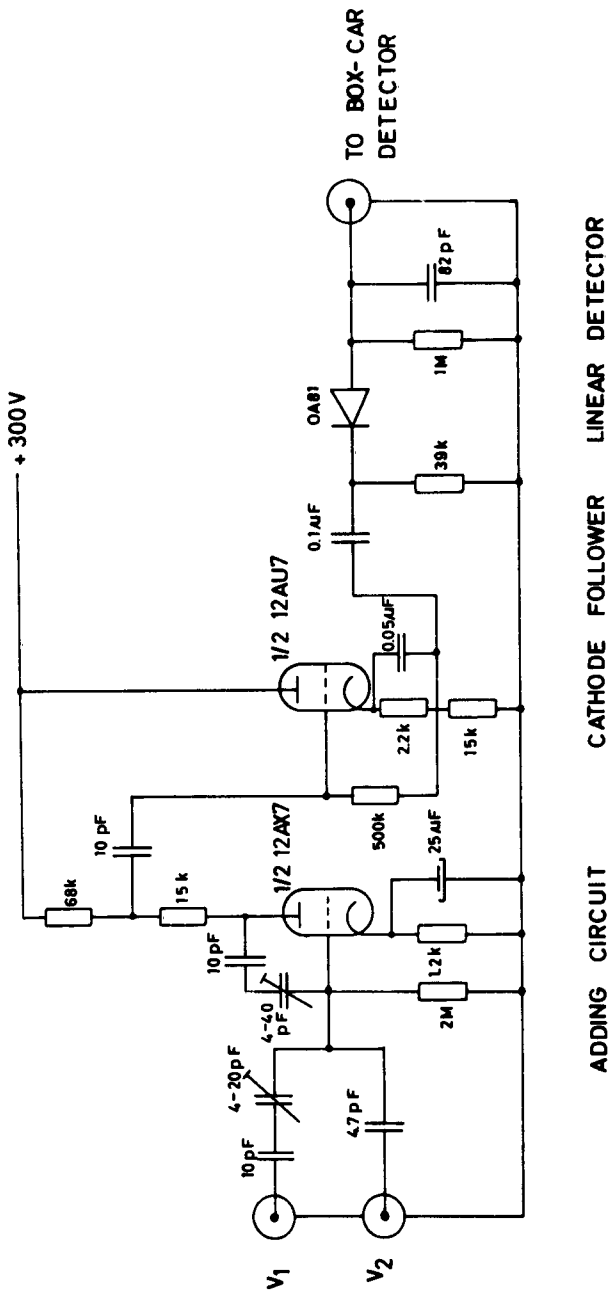

Diagram 5.2 Adding circuit and linear detector

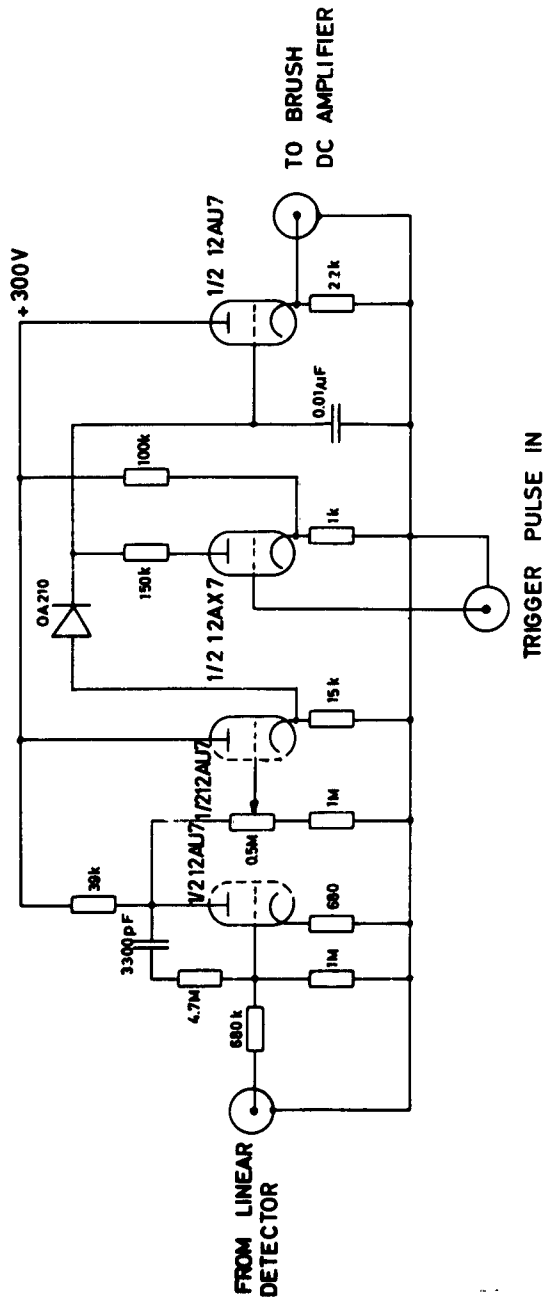

Diagram 5.3 Box car detector

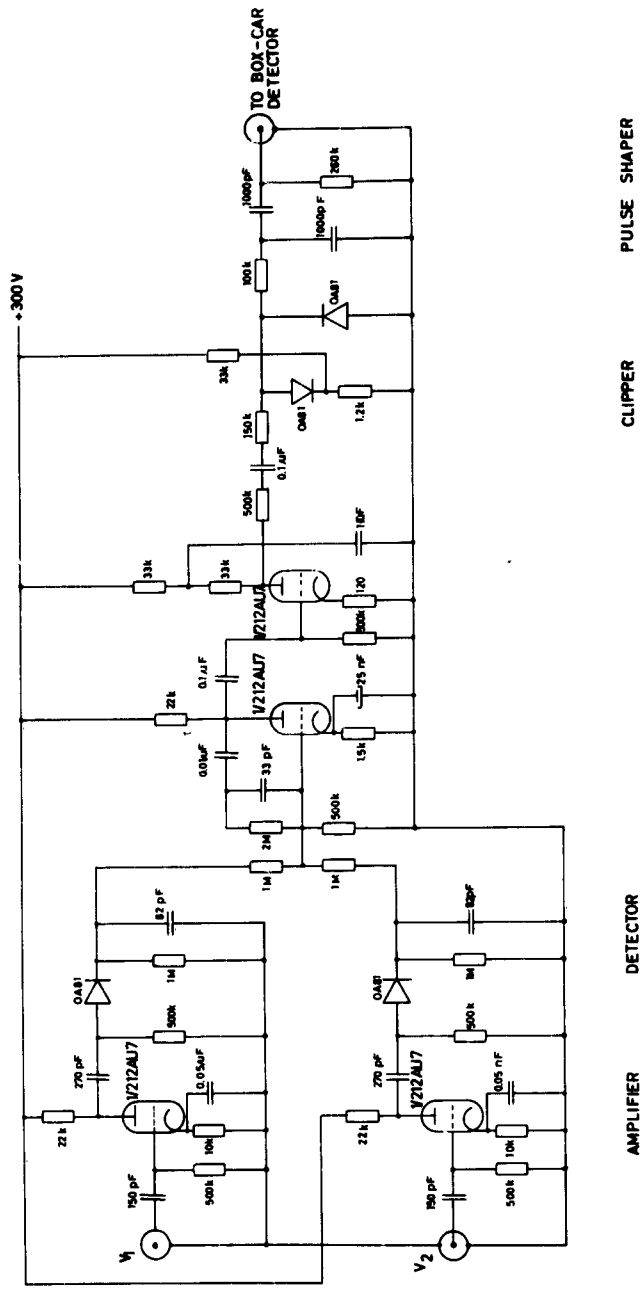

Diagram 5.4 Trigger pulse circuit

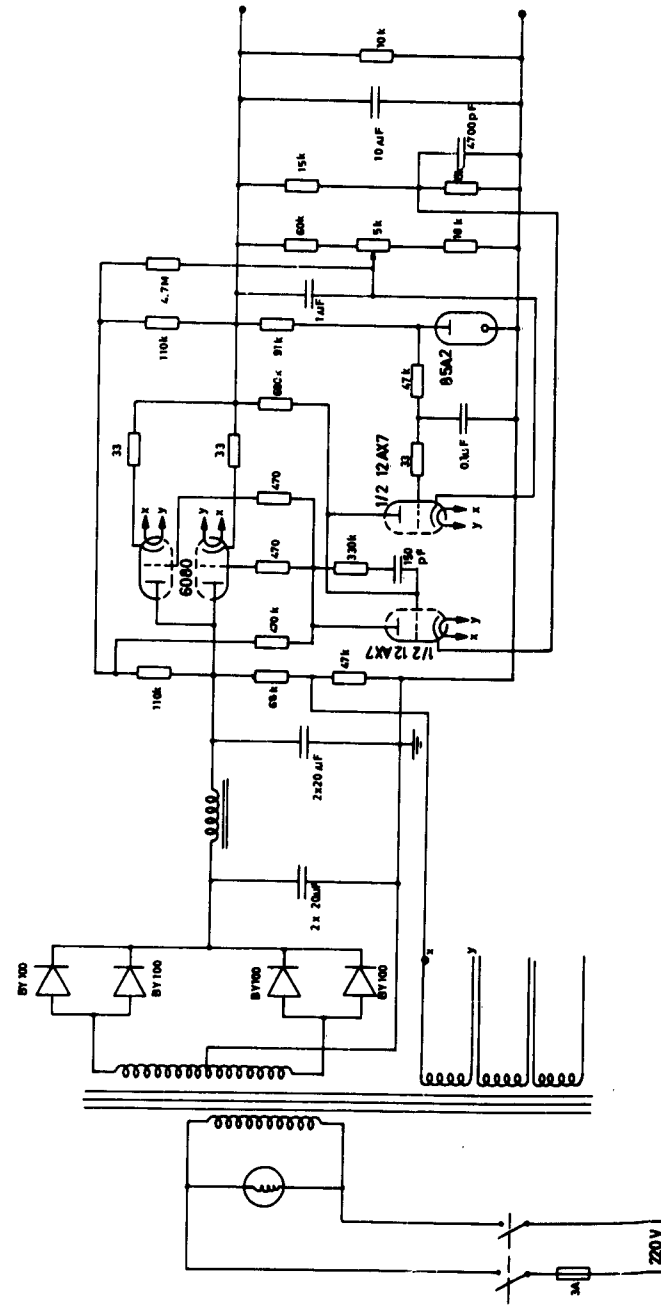

Diagram 5.5 Power supply

NORW DEFENCE
RESEARCH ESTABL
KJELLER, NORWAY

AF 61(052)-500
TR
GEOPHYSICS

NDRE REPORT No 45
10 March 1963

A STUDY OF IONOSPHERIC IRREGULARITIES

P CHRISTOPHERSEN
T HAGFORS
H BØEN

ABSTRACT: Irregular structure and irregular motions in the F-layer of the ionosphere are investigated through the study of the correlation between radio waves reflected at closely spaced frequencies. The frequency range over which correlation remains is highly variable and lies between 10 and 100 kc/s.

NORW DEFENCE
RESEARCH ESTABL
KJELLER, NORWAY

AF 61(052)-500
TR
GEOPHYSICS

NDRE REPORT No 45
10 March 1963

A STUDY OF IONOSPHERIC IRREGULARITIES

P CHRISTOPHERSEN
T HAGFORS
H BØEN

ABSTRACT: Irregular structure and irregular motions in the F-layer of the ionosphere are investigated through the study of the correlation between radio waves reflected at closely spaced frequencies. The frequency range over which correlation remains is highly variable and lies between 10 and 100 kc/s,

NORW DEFENCE
RESEARCH ESTABL
KJELLER, NORWAY

AF 61(052)-500
TR
GEOPHYSICS

NDRE REPORT No 45
10 March 1963

A STUDY OF IONOSPHERIC IRREGULARITIES

P CHRISTOPHERSEN
T HAGFORS
H BØEN

ABSTRACT: Irregular structure and irregular motions in the F-layer of the ionosphere are investigated through the study of the correlation between radio waves reflected at closely spaced frequencies. The frequency range over which correlation remains is highly variable and lies between 10 and 100 kc/s.

NORW DEFENCE
RESEARCH ESTABL
KJELLER, NORWAY

AF 61(052)-500
TR
GEOPHYSICS

NDRE REPORT No 45
10 March 1963

A STUDY OF IONOSPHERIC IRREGULARITIES

P CHRISTOPHERSEN
T HAGFORS
H BØEN

ABSTRACT: Irregular structure and irregular motions in the F-layer of the ionosphere are investigated through the study of the correlation between radio waves reflected at closely spaced frequencies. The frequency range over which correlation remains is highly variable and lies between 10 and 100 kc/s.